Journal of Hydrology: Regional Studies 52 (2024) 101717

Contents lists available at ScienceDirect

Journal of Hydrology: Regional Studies

journal homepage: www.elsevier.com/locate/ejrh

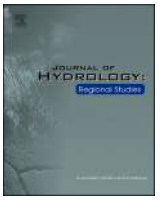

Analysis of SPI index trend variations in the United Kingdom - A cluster-based and bayesian ensemble algorithms approach

Fabio Di Nunno, Giovanni de Marinis, Francesco Granata *

University of Cassino and Southern Lazio, Department of Civil and Mechanical Engineering (DICEM), Via Di Biasio, 43, Frosinone, Cassino 03043, Italy

ARTICLE INFO

Keywords:
Drought
SPI
Clustering
Changepoint detection
United Kingdom

ABSTRACT

Study region: United Kingdom (UK).
Study focus: A regional investigation of the Standard Precipitation Index (SPI) trends and abrupt changes in the UK has been carried out. The K-means algorithm was employed to partition the study area into six homogeneous regions, each distinguished by specific SPI characteristics. Subsequently, the seasonal Mann-Kendall (MK) test and the Bayesian Changepoint Detection and Time Series Decomposition (BEAST) algorithm were used to evaluate the overall trends for each cluster and SPI time scale, as well as to identify abrupt changes in trend and seasonality along the SPI time series, respectively.
New hydrological insights for the region: The seasonal MK test revealed statistically significant increasing SPI trends for all clusters, except for the southeastern area of the UK, where decreasing, but not statistically significant, SPI trends were observed. Moreover, despite a scenario suggesting an increasingly humid UK, the BEAST analysis allowed the detection of decreasing abrupt changes in trends, resulting in sudden changes from wet to dry conditions, that cannot be identified using the MK test. Alongside these, the BEAST analysis has also revealed positive abrupt changes in trends across all UK, as well as positive or negative variations in seasonality, which are followed by longer or shorter wet or dry periods, respectively. Overall, the study approach provides a detailed picture of the SPI trends and abrupt changes, in light of the impact of climate change on the different areas of the UK.

1. Introduction

Drought stands out as one of the most complex phenomena among all extreme climatic events (Dadson et al., 2019). Its complexities stem from the significant challenges in assessing how the duration and severity of drought events can change over time. These changes arise due to various hydrological, climatic, and socio-economic factors affecting different regions worldwide in more or less distinct ways (Roushangar and Ghasempour, 2021). Moreover, drought events typically give rise to numerous adverse effects that can significantly impact various sectors. Specifically, the decrease in water levels in rivers, natural water bodies, and man-made reservoirs during drought periods can lead to the degradation of aquatic habitats. Additionally, it results in a scarcity of water for irrigation, livestock, and human consumption, causing serious repercussions in the socio-economic sphere. This is even more true in the context of climate change, with the frequency and intensity of drought events increasing due to global warming, leading to significant

* Corresponding author.
E-mail addresses: fabio.dinunno@unicas.it (F. Di Nunno), demarinis@unicas.it (G. de Marinis), f.granata@unicas.it (F. Granata).

https://doi.org/10.1016/j.ejrh.2024.101717
Received 14 October 2023; Received in revised form 16 February 2024; Accepted 22 February 2024

List of Symbols

AC_{season}	Abrupt change in seasonality
AC_{trend}	Abrupt change in trend
A_i	Clustering - Set of points related to the i-th cluster
BA	Bayesian Approach
BEAST	Bayesian Changepoint Detection and Time Series Decomposition
C1	Cluster C1
C2	Cluster C2
C3	Cluster C3
C4	Cluster C4
C5	Cluster C5
C6	Cluster C6
DWT	Discrete Wavelet Transform
EEMD	Ensemble Empirical Mode Decomposition
EMD	Empirical Mode Decomposition
IDW	Inverse Distance Weighting
IHU	Integrated Hydrological Unit
J(X;V)	Clustering - Distance between two clusters
K-means	K-means clustering algorithm
$M = \{AC_{trend}, AC_{season}, \delta^2\}$	BEAST Analysis - Unknown parameters
MCMC	Markov Chain Monte Carlo
MK	Mann-Kendall
MODIS	Moderate resolution imaging spectroradiometer
MODWT	Maximal Overlap Discrete Wavelet Transform
$N(0, \delta^2)$	BEAST Analysis - Gaussian random error term
Ncp_{season}	Mean number of changepoints in seasonality
Ncp_{trend}	Mean number of changepoints in trend
Ni	Clustering - Point related to the i-th cluster
PCA	Principal Component Analysis
PDSI	Palmer Drought Severity Index
Pr(scp)	Probability of season changepoint
$PR_{ncp\text{-}10\%}$	The 10% from the probability distribution for number of changepoints
$PR_{ncp\text{-}90\%}$	The 90% from the probability distribution for number of changepoints
$PR_{ncp\text{-}mode}$	The mode from the probability distribution for number of changepoints
p-value	Seasonal MK - Significance Level
R^2	Coefficient of determination
RMSE	Root mean square error
S	BEAST Analysis - Season
scPDSI	Self-calibrating Palmer Drought Severity Index
scPDSIx	Multiscalar self-calibrating Palmer Drought Severity Index
SPEI	Standardized Precipitation Evapotranspiration Index
SPI	Standard Precipitation Index
SPTI	Standardized Precipitation Temperature Index
T	BEAST Analysis - Trend
V	Clustering - Centers of the c clusters
UK	United Kingdom
VHI	Vegetation health index
v_i	Clustering - i-th cluster center
$x_k^{(i)}$	Clustering - k-th data belonging to the i-th cluster
Y(t)	BEAST Analysis - Time Series
z	Mean elevation of each hydrological unit
Z	Seasonal MK - Test Statistic
β	Seasonal MK - Sen's Slope
δ^2	BEAST Analysis - Variance
ε	BEAST Analysis - Noise
σ^2	Variance of error

socio-economic and ecological losses (Wu et al., 2022). Hence, precisely characterizing the spatio-temporal trends and changes in drought can help mitigate vulnerability and enhance the management of drought-prone activities (Ghasempour et al., 2022).

In literature, various synthetic indices for drought monitoring have been introduced. The SPI (McKee et al., 1993) stands out as the most commonly used drought index, offering a characterization of both short- and long-term drought based solely on precipitation time series. Other indices, such as the Standardized Precipitation Evapotranspiration Index (SPEI, Vicente-Serrano et al., 2010) and Standardized Precipitation Temperature Index (SPTI, Ali et al., 2017), also exist but require temperature data, which may not always be available for extended periods, hindering their applicability in characterizing droughts. The Palmer Drought Severity Index (PDSI, Palmer, 1965) is another drought index that relies on a soil-water balance equation, considering factors like precipitation, moisture supply, runoff, and evaporation demand at the surface level. However, the PDSI has several drawbacks. PDSI is highly sensitive to temperature variations, with temperature that influences evaporation rates and, consequently, the overall soil-water balance, leading to potential inaccuracies in drought severity assessments. PDSI's performance can be constrained also by the calibration period used in its computation. The fixed calibration period may not adequately capture changing climate patterns, limiting the index's ability to adapt to evolving hydrological conditions. In addition, PDSI operates on a fixed temporal scale, which might not effectively capture drought events occurring at various time scales. This limitation can result in a lack of flexibility when identifying and characterizing drought conditions over different durations. To address these limitations, Wells et al. (2004) proposed a self-calibrating version of the PDSI, known as scPDSI, which dynamically calculates PDSI constants based on station-specific features, enhancing its spatial comparability. Furthermore, Liu et al. (2017) introduced a multiscalar version, scPDSIx, capable of identifying drought at different time scales. The scPDSIx, with its multiscalar capabilities, allows for a more comprehensive assessment of drought conditions by capturing short-term, medium-term, and long-term variations. This ensures a nuanced understanding of the evolving drought scenario. However, despite its advantages, the computation of the scPDSIx index is complex, posing challenges to its practical application (Zhang et al., 2021).

An intriguing aspect of investigating drought phenomena lies in understanding their spatial distribution, often addressed through the identification of homogeneous drought regions via a clustering process. Yoo et al. (2012) employed the widely used K-means clustering algorithm to study drought in South Korea. They incorporated regional drought features such as frequency, duration, and severity into the clustering process. The study revealed insights into how drought manifests across different regions in South Korea. In a different study, Li et al. (2013) investigated drought in the Lancang River Basin, China, by applying both the K-means algorithm and Principal Component Analysis (PCA). The temporal variability of droughts was explored using Empirical Mode Decomposition (EMD) analysis and the wavelet method. The authors found that PCA and K-means consistently divided the Lancang River basin into four zones, indicating a robust relationship between climate and drought features. Guo et al. (2018) utilized PCA to assess sub-regional drought patterns in Central Asia, based on SPEI data at different time scales. They combined PCA with the Varimax rotation method to identify more stable localized drought patterns than with individual PCA analysis. This approach enhanced the understanding of the spatial distribution of drought in Central Asia. Aladaileh et al. (2019) employed a different clustering algorithm, the Hierarchical one, to investigate the spatial extent of drought events in Jordan. They based their analysis on the Standardized Precipitation Index (SPI) computed from various meteorological stations at 3, 6, and 12-month time scales, providing insights into the spatial characteristics of drought events in the region. Similarly, Neto et al. (2021) applied the Hierarchical clustering algorithm to identify homogeneous drought zones in Paraiba State, Brazil. They considered the SPI index over a broader range of time scales, from 1 to 48 months, and grouped the zones based on drought state, duration, and severity. This study contributed to a comprehensive understanding of drought patterns in Paraiba State. In the analysis of drought in northwestern Iran, Roushangar and Ghasempour (2021) proposed a hybrid method that combined temporal preprocessing and spatial classification. They utilized gridded SPEI data from 60 points covering northwestern Iran and applied the Maximal Overlap Discrete Wavelet Transform (MODWT) to extract time-series time-frequency attributes. Based on the outcomes of the MODWT, the clustering was carried out using the K-means algorithm, dividing the study area in five different clusters, each characterized by different values of mean SPEI variation and energy variation. Building on this approach, Ghasempour et al. (2022) introduced an intermediate step between MODWT and K-means. They incorporated Ensemble Empirical Mode Decomposition (EEMD) for further decomposition, aiming to achieve more stationary time series before applying the K-means clustering algorithm. This additional step, represented by the EEMD, aimed to enhance the effectiveness of the clustering process by addressing potential non-stationarities in the data. In a more recent study, Derradji et al. (2023) focused on spatiotemporal drought monitoring in the Mediterranean area of Northeastern Algeria. They employed the vegetation health index (VHI) derived from moderate resolution imaging spectroradiometer (MODIS) data. Utilizing the K-means algorithm, the researchers partitioned the study area into three clusters: northern, central, and southern zones. Notably, the northern and central areas, located closer to the coast, exhibited no signs of drought. In contrast, the southern region experienced prolonged periods of drought, ranging from mild to moderate severity. This research provided valuable insights into the varying drought conditions across different zones in Northeastern Algeria. Furthermore, Di Nunno and Granata (2023a) introduced a novel approach combining clustering and forecasting for investigating drought in the Mediterranean area of Southern Italy. They utilized gridded data of the SPEI with a forecasting time scale of 6 months. Artificial Intelligence algorithms were incorporated into their methodology. The authors tested various clustering algorithms, including K-means, Hierarchical, and Expectation-Maximization, revealing five distinct clusters characterized by drought events of varying duration and severity. This combined approach not only focuses on the spatial distribution of drought but also incorporates forecasting elements, allowing for a proactive understanding of drought trends in the Mediterranean region of Southern Italy. The utilization of Artificial Intelligence algorithms enables a more comprehensive and nuanced exploration of drought dynamics in the area. The identification of distinct clusters based on duration and severity contributes to a refined understanding of the temporal aspects of drought events, emphasizing the significance of evaluating both spatial distribution and temporal trends in drought investigation.

In addition to assessing the spatial distribution of drought phenomena across different temporal scales, the evaluation of drought trends holds significant importance in decision-making for implementing necessary precautions. Understanding drought severity and identifying its trend can provide valuable insights for planning and managing water resources and agricultural areas. Researchers worldwide often explore various methodologies for analyzing drought trends. For instance, Zhang et al. (2012) conducted an evaluation of drought events in Xinjiang, China, based on the Standardized Precipitation Index (SPI). They started from the daily precipitation data for 1957–2009 from 53 stations, employing the MK trend test (Mann, 1945, Kendall, 1948) on the computed monthly scale time series to detect trends in SPI, contributing to a comprehensive understanding of drought dynamics in the region. The authors observed diverse trends across the investigated territory. For instance, they noted a decline in the occurrence of droughts in North Xinjiang during winter, but a drying trend throughout spring, summer, and autumn, which could potentially threaten agriculture. In a more recent study, Khan et al. (2021) conducted a spatio-temporal analysis of rainfall and drought conditions in Southwest Xinjiang. Utilizing the SPI index and the MK test, they revealed a decreasing rainfall trend and an increasing drought trend, which may further endanger the region's flora and fauna. Additionally, Gumus et al. (2021) proposed a spatio-temporal analysis of drought in the Southeastern Anatolia Project (GAP) region in Turkey. Their analysis was based on the SPI at different time scales, the MK test, and Sen's Slope method (Sen, 1968). Uniquely, they also incorporated the 'pre-whitened' method to remove serial correlation from the time series before analysis. The authors identified a declining and statistically significant trend in 30% of the examined stations for the 12-month SPI. Furthermore, they conducted a spatial analysis using the Inverse Distance Weighting (IDW) method, contributing to a comprehensive understanding of drought patterns in the region.

It must be noted that while the MK test is a reliable tool for analyzing trends in hydrological variables, it has certain limitations. The primary constraint of the MK test lies in its focus on monotonic trends, rendering it less suitable for detecting more complex patterns in the data. Consequently, the MK test does not facilitate the analysis of changepoints and seasonality in trends. The implications of this limitation are significant. For instance, an abrupt transition from a dry spell to a period of heavy rain can cause flooding, as soil that has been dry for an extended period may struggle to absorb the sudden excess water. Conversely, a rapid shift from wet to dry conditions can trigger droughts, severely impacting water supply. Additionally, these sudden changes in weather patterns can be detrimental to agricultural systems. For example, if a drought strikes unexpectedly during a critical growth phase of crops, it could lead to crop failure, thus affecting food production and security.

In the literature, various changepoint tests have been reported, as documented by Reeves et al. (2007). These tests encompass rank tests for changepoint problems, as introduced by Lombard (1987), and parametric tests exemplified by Jarušková (1997). Despite the diversity of available tests, the Pettitt test (Pettitt, 1979) emerges as the most extensively utilized in the realm of time series analysis. Notably, it has found applications across a broad spectrum of hydroclimatic time series, as evidenced by studies conducted by Abahous et al. (2018), Bosneagu et al. (2022), and Gholami et al. (2022). An alternative approach to addressing the changepoint problem is through the Bayesian Approach (BA). Zerouali et al. (2023) have applied a model that combines BA with the discrete wavelet transform (DWT) to discern changepoints in the monsoon rainfall of the Narmada River, India, spanning the years 1901 to 2015. The BA-DWT analysis reveals a shift towards drier conditions commencing in the 1960 s, with a long-term trend originating as far back as the 1920 s. In addition to BA-DWT, another noteworthy Bayesian-based method is the BEAST, developed by Zhao et al. (2019) for analyzing satellite remote sensing data. The BEAST stands out for its capability to concurrently identify abrupt changes, seasonal variations, and trends, while also accommodating non-linear trends within time series. This method has found valuable applications in diverse fields, including the monitoring of vegetation dynamics in lakes (Cai et al., 2020), modeling dam displacement (Xu et al., 2022), and analyzing trends in groundwater levels (Keerthana and Nair, 2022), as well as streamflow rates (Sakizadeh et al., 2023). Overall, the literature encompasses a range of changepoint tests, with the Bayesian approaches, such as BA-DWT and BEAST, being proposed as alternative methodologies, demonstrating their versatility in addressing changepoint problems across various environmental contexts.

In the present study, a combined clustering and change point detection approach was proposed for the drought analysis in the UK. The BEAST was applied for the drought analysis in the UK, identifying changepoints in trends and seasonality along the SPI time series at time scales 1, 3, 6, 12 and 24 months. Then, based on the parameters evaluated using the BEAST algorithm, the K-means clustering algorithm was used to identify homogenous SPI regions and the seasonal MK test was applied to assess the overall trends of the SPI, for each cluster and time scale. Overall, the integration of the BEAST algorithm for the drought temporal analysis and the K-means clustering algorithm for spatial clustering forms a synergistic approach, enhancing the understanding of UK drought dynamics. BEAST's identification of temporal changepoints at multiple scales contributes information on the changing nature of drought over time. Meanwhile, K-means clustering uses BEAST-derived parameters to classify regions with similar drought patterns, offering a spatial dimension. Together, these methodologies create a holistic understanding, linking temporal and spatial perspectives and facilitating more informed and targeted strategies for drought management in the UK.

Furthermore, the SPI was chosen as drought index for its simplicity and flexibility. Its computation requires the only precipitation data, making it accessible in regions with limited meteorological information. Its adaptability to various temporal scales enables a comprehensive assessment of drought severity over different periods. However, the SPI has limitations, being based on the only precipitation, overlooking factors like temperature and soil moisture, which were instead include in more complexes SPEI and scPDSIx indices.

To the authors' knowledge, no previous study has investigated points of change in drought patterns using the BEAST algorithm. Therefore, the implementation of the combined changepoint sensing and clustering approach is definitely novel and has never proposed in literature so far, even for other hydrological applications. This approach is particularly interesting in the context of climate change. The outcomes obtained from the present study were critically analyzed, aiming to provide valuable insights for:

- the management of water resources, since the detection of abrupt variations in trends and seasonality may help resource managers anticipate changes, plan for water allocation, and implement adaptive strategies to mitigate the effects of drought;
- the planning of new infrastructures, like reservoirs, irrigation systems, and water distribution networks, could adapt to changing hydrological patterns;
- agricultural decisions, since sudden changes in drought patterns can disrupt agricultural cycles, affecting crop yields and quality, the early detection of abrupt changes may help farmers adapt their strategies.
- early warning systems, when sudden changes are detected and expected, the authorities may alert the affected regions, activating timely responses and preventive measures.

2. Materials and methods

2.1. Dataset

The UK is characterized by a temperate climate with generally cool temperatures and abundant rainfall throughout the year. The temperature variations follow a moderate range, rarely dropping below 0 °C or exceeding 30 °C (86 °F). Inland areas, specifically upland regions of England, Wales, Northern Ireland, and much of Scotland, encounter an oceanic climate. Higher mountainous areas in Scotland have a continental subarctic climate. The prevailing wind in the UK originates from the southwest, leading to frequent rainfall from the Atlantic Ocean. Consequently, the western regions receive more precipitation, driven by the warmth of the Gulf Stream that influences the Atlantic currents. This contributes to milder winters, particularly in the west, where winters are wetter, especially in highland areas. On the other hand, the eastern parts of the UK are mostly shielded from this wind influence, resulting in drier conditions. Summers are warmest in the southeast of England and coolest in the north. In winter and early spring, heavy snowfall is possible on high ground, and occasionally, significant snow accumulations occur away from the hills.

For the current study, the SPI data from 115 hydrological units covering the UK territory were used, at time scales of 1, 3, 6, 12, 18, and 24 months (details at https://eip.ceh.ac.uk/hydrology/water-resources). The SPI data covered the period from January 1862 to September 2022.

SPI values at different time scales were computed, as originally defined in McKee et al. (1993), starting from a 5 km gridded monthly precipitation dataset generated by the United Kingdom Met Office through an extensive data rescue and digitization initiative conducted within the framework of the Historic Droughts project (grant number: NE/L01016X/1). Dataset was constructed using a methodology consistent with the UKCP09 data, with the interpolation process that employed the IDW technique as outlined by Perry and Hollis (2005). Notably, each pixel within the gridded dataset corresponds to the precipitation value at the center of the respective cell, ensuring a spatially accurate representation of precipitation patterns over the specified period. These grids were area-averaged over each Integrated Hydrological Unit (IHU) Hydrometric Area, as outlined by Kral et al. (2015). In this version of the dataset (version 2), the monthly rainfall grids from 1960 to 2000 were derived from the Met Office 5-km daily rainfall grids to address some localized issues identified in the Met Office monthly rainfall grids (Hollis et al., 2019).

It must be pointed out that the Met Office dedicated substantial efforts to digitizing precipitation data dating back to the latter half of the 19th century as part of the Historic Droughts project. This undertaking markedly augmented the density of the monthly rain gauge network, particularly during the earlier timeframe from 1862 to 1910. In comparison with the rain gauge density utilized in deriving alternative datasets like the CEH-GEAR rainfall datasets (Keller et al., 2015; Tanguy et al., 2019), this initiative has significantly enhanced the precision of the historical data. The data rescue and digitization program, conducted by the Met Office between 2019 and 2020, introduced over 200 additional monthly gauges into the network for the period spanning 1862 to 1910. Despite these commendable efforts, the reliability of the data, especially pertaining to the earlier years, necessitates cautious consideration. In-depth descriptions of the uncertainties and homogeneity of the dataset were also provided by Tanguy et al. (2021) and Hollis et al. (2019), respectively.

In order to compute the SPI at different time scales, the rainfall data were fitted to a statistical distribution. In this dataset, the chosen statistical distribution was the gamma distribution, widely used and recommended as a default for Europe by Stagge et al. (2015). The L-moments method was applied to estimate the gamma distribution parameters, as the Maximum Likelihood method encountered difficulties in fitting a realistic distribution in some isolated cases (Tanguy et al., 2017). For SPI calculation, the R package SCI was used, modified to employ L-moments instead of Maximum Likelihood.

Table 1
SPI index categories. Colorbar ranges from red (low values) to green (high values).

Categories	SPI Values
Extreme drought	Lower than -2.00
Severe drought	-1.99 to -1.50
Moderate drought	-1.49 to -1.00
Near normal	-0.99 to 0.99
Moderately wet	1.00 to 1.49
Severely wet	1.50 to 1.99
Extremely wet	Higher than 2.00

It is important to note that the SPI index enables the assessment of both short- and long-term drought effects, as it can be calculated at various time scales. Typically, for monitoring agriculture and meteorological droughts, 3- or 6-month scales are used, while higher time scales, such as 12 and 24 months, are considered for analyzing hydrological drought and socioeconomic impact, respectively (Tan et al., 2015). Furthermore, the SPI allows for the classification of the degree of dryness or wetness, ranging from extreme drought, SPI lower than −2, to extremely wet conditions, SPI higher than 2 (Table 1, Costa., 2011).

2.2. BEAST

The BEAST algorithm decomposes a time series Y(t) into the following distinct components: trend (T), seasonal variability (S), abrupt changes (AC_{trend} and AC_{season}), and noise (ε). These components are combined additively to model the time series (Hu et al., 2021):

$$Y(t) = T(AC_{trend}) + S(AC_{season}) + \varepsilon \tag{1}$$

where ε is the Gaussian random error term N(0, δ^2) with unknown variance δ^2. T and S represent the fundamental terms for the trend and seasonality components, respectively, and they implicitly encapsulate abrupt changes through the parameters AC_{trend} and AC_{season}. Specifically, AC_{trend} and AC_{season} denote the numbers and locations of changepoints in the trend and seasonal components. The Bayesian theorem is utilized to determine the unknown parameters $M = \{AC_{trend}, AC_{season}, \delta^2\}$ as a posterior probability distribution through simulation using Markov Chain Monte Carlo (MCMC) sampling. MCMC is a computational method used for sampling from complex probability distributions, particularly in Bayesian statistics. The goal of MCMC is to approximate the posterior distribution of a set of unknown parameters given observed data. The process is as follows:

$$f(M|Y) \propto f(Y|M) * f(M) \tag{2}$$

The posterior probability, denoted as f(M|Y), encapsulates comprehensive information about the time series decomposition, encompassing details such as the counts and positions of changepoints within the trend and seasonal components. However, obtaining an analytical solution for f(M|Y) is impractical due to its intricate nature, necessitating stimulation through the MCMC sampling method. However, for a detailed understanding of the theoretical aspects, please refer to the original reference paper (Zhao et al., 2019). In this study, the BEAST algorithm is used to detect changepoints in both trend and seasonality within the SPI time series across various time scales, as well as to estimate the abrupt changes associated with these components.

2.3. Clustering

Clustering is a classification process that divides a large set of data into a smaller number of groups. The purpose of clustering is to group similar data points together, forming clusters where the data within each cluster shares common features, while data in different clusters exhibit some heterogeneity (Di Nunno and Granata 2023a, 2023b).

For the present study, the K-means algorithm was employed to divide UK into homogeneous areas. The clustering process starts by treating each observation as an individual cluster. It then iteratively proceeds with two steps: identifying the pair of closest clusters and merging them based on a specified linking criterion. This process continues until all clusters are eventually merged. The distance between two clusters is measured using the Manhattan distance formula:

$$J(X;V) = \sum_{i=1}^{c} \sum_{k \in i} \left| x_k^{(i)} - v_i \right| \tag{3}$$

where $V = \{v_i \mid i = 1, \ldots, c\}$ are the centers of the c clusters, $x_k^{(i)}$ is the k^{th} data point belonging to the i^{th} cluster, and $x_k^{(i)} - v_i$ is the distance between each data point and his cluster center v_i. Each cluster center was computed as:

$$v_i = \frac{\sum_{k=1}^{N_i} x_k}{N_i}, x_k \in A_i \tag{4}$$

where A_i is the set of points N_i related to the i^{th} cluster. Thus, the Manhattan distance measures the distance between two points by summing up the absolute differences of each variable pair (Callahan and Bridge, 2021). In contrast, alternative distance formulations, like the Euclidean distance, sum up the squared differences of each variable. As a result, two data points may have similarity in most variables but differ significantly in one. In such a case, the assessment of Euclidean distance may be overly influenced by this single difference. On the contrary, the Manhattan distance will be more influenced by the similarity of the other variables, making it more robust and less susceptible to the impact of outliers (Di Nunno et al., 2023c). Furthermore, it should be noted that the optimal number of clusters is not known beforehand. Hence, a preliminary analysis based on the Silhouette technique was performed to assess the proper clustering with the optimal set of input parameters (more details in Section 2.4). Specifically, the Silhouette score ranges from −1, indicating a wrong cluster assignment, to 1, indicating that the clusters are well-defined and distinct from each other. Silhouette scores close to 0 suggest a non-significant distance between the clusters. The software used for the clustering procedure was Orange (Demsar et al., 2013).

2.4. Modeling procedure

The modeling (depicted in Fig. 1) consisted of the integrated use of BEAST, K-means, and seasonal MK algorithms, as outlined in the subsequent procedure:

1. The BEAST algorithm was employed to detect changepoints in both trend and seasonality in the time series of the SPI at various time scales. As input for the subsequent clustering (Step 2), various BEAST parameters were initially considered for each hydrological unit. These parameters were computed for each twenty-years period from 1860–1880 to 2000–2020 and covered all SPI time scales. The analysis includes the mean number of changepoints in trend and seasonality (Ncp_{trend} and Ncp_{season}, respectively), as well as the minimum, mean and maximum values of abrupt change in trend and seasonality (AC_{trend} and AC_{season}, respectively). It is important to note that the decision to compute the BEAST variables based on a twenty-year temporal window was made to conduct a comprehensive examination of the distribution of changepoints in trend and seasonality across the time series, while also assessing their magnitude. A smaller time window, such as 5 or 10 years, would result in a considerable reduction or even a lack of changepoints within each window. Conversely, a larger time window, such as 50 years, would not accurately capture the historical moments when the changepoints occurred. However, other BEAST parameters computed for the entire time series were also included in the clustering process. These parameters include the variance of error (σ^2), the root mean square error (RMSE), the coefficient of determination (R^2), the mode from the probability distribution for number of changepoints ($PR_{ncp\text{-}mode}$) and the 10% and 90% from the probability distribution for number of changepoints ($PR_{ncp\text{-}10\%}$ and $PR_{ncp\text{-}90\%}$, respectively). Finally, the elevation (z) of each hydrological unit was also included in the clustering process.
2. The K-means clustering algorithm was employed to identify homogenous SPI regions based on the parameters evaluated using the BEAST algorithm. The analysis of results involved comparing the different clusters that were detected based on the optimal set of input variables, as determined by the Silhouette score (see Section 2.3). The focus was on the SPI statistics at various time scales.
3. The seasonal MK test was employed to assess the overall trends of SPI across different time scales, based on the mean SPI time series computed for each cluster detected with the K-means clustering algorithm. It is important to acknowledge that the SPI time series might exhibit varying seasonal patterns. As an alternative to the traditional MK test, the seasonal MK test has been implemented, which takes into consideration the seasonality when estimating the MK parameters. The latter are mainly represented by Z, which is used to detect a statistically significant trend, based on a confidence level that has been settled equal to the 5% according the previous literature studies. The Z statistic is a measure of how many standard deviations a data point is from the mean. Its sign indicates the direction of the trend, positive for an increasing trend and negative for a decreasing trend. The Sen's slope β applied to evaluate the linear trend slope. Sen's slope is calculated by determining the median of all possible slopes between pairs of data points. Therefore, positive and negative β values indicate increasing and decreasing trends, respectively. A complete description of the seasonal MK test was provided by Hirsch and Slack (1984) and Di Nunno et al. (2023c).
4. Finally, the BEAST analysis results were examined, assessing mean values of changepoints and abrupt change magnitudes for trends and seasonality in each cluster and SPI time scale. The analysis involved the representation of different BEAST plots, illustrating the trends and seasonal features for different reference hydrological units.

3. Results

3.1. Clustering

The optimization of the number of clusters and of the proper subset of input variables was performed based on the Silhouette technique (see Sections 2.3 and 2.4). As shown in Table 2, the best mean Silhouette score, equal to 0.621, was obtained for a number of clusters equal to 6 and assuming as input variables the mean number of Ncp_{trend} and Ncp_{season}, along with the minimum, mean and maximum values of AC_{trend} and AC_{season}, computed for each twenty-year period. Additionally, Tables 3 and 4 present the average values of the SPI statistics. These averages are calculated across the different time scales for each cluster (Table 3). Table 4, on the other hand, provides the SPI statistics for the various time scales and clusters. Moreover, Figs. 2 and 3 illustrate the Silhouette scores for all hydrological units related to the six clusters, and a representation of the SPI clustering of the UK, respectively. Below is provided a

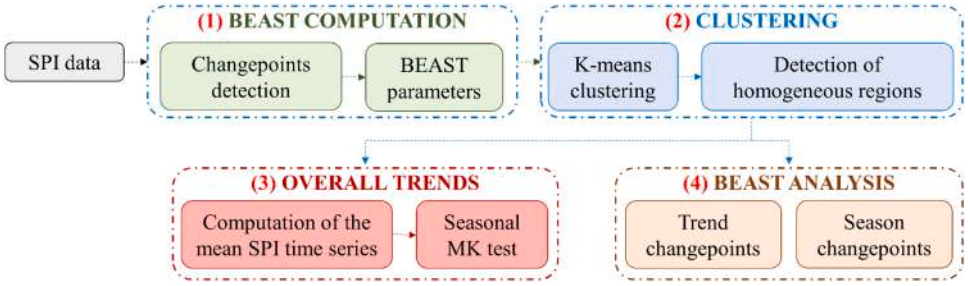

Fig. 1. Flowchart of the modeling procedure.

Table 2
Mean Silhouette scores for different number of clusters and subsets of input variables (in bold the best value). Colorbar ranges from red (low values) to green (high values).

Input variables	Number of Clusters						
	2	3	4	5	6	7	8
$Ncp_{trend(1860\text{-}1880)}$, $Ncp_{trend(1880\text{-}1900)}$, $Ncp_{trend(1900\text{-}1920)}$, $Ncp_{trend(1920\text{-}1940)}$, $Ncp_{trend(1940\text{-}1960)}$, $Ncp_{trend(1960\text{-}1980)}$, $Ncp_{trend(1980\text{-}2000)}$, $Ncp_{trend(2000\text{-}2020)}$	0.602	0.577	0.57	0.596	0.607	0.600	0.584
$Ncp_{season(1860\text{-}1880)}$, $Ncp_{season(1880\text{-}1900)}$, $Ncp_{season(1900\text{-}1920)}$, $Ncp_{season(1920\text{-}1940)}$, $Ncp_{season(1940\text{-}1960)}$, $Ncp_{season(1960\text{-}1980)}$, $Ncp_{season(1980\text{-}2000)}$, $Ncp_{season(2000\text{-}2020)}$							
$AC_{trend(1860\text{-}1880)}$, $AC_{trend(1880\text{-}1900)}$, $AC_{trend(1900\text{-}1920)}$, $AC_{trend(1920\text{-}1940)}$, $AC_{trend(1940\text{-}1960)}$, $AC_{trend(1960\text{-}1980)}$, $AC_{trend(1980\text{-}2000)}$, $AC_{trend(2000\text{-}2020)}$							
$AC_{season(1860\text{-}1880)}$, $AC_{season(1880\text{-}1900)}$, $AC_{season(1900\text{-}1920)}$, $AC_{season(1920\text{-}1940)}$, $AC_{season(1940\text{-}1960)}$, $AC_{season(1960\text{-}1980)}$, $AC_{season(1980\text{-}2000)}$, $AC_{season(2000\text{-}2020)}$							
z, σ^2, RMSE, R^2, $PR_{ncp\text{-}mode}$, $PR_{ncp\text{-}10\%}$, $PR_{ncp\text{-}90\%}$,							
$Ncp_{trend(1860\text{-}1880)}$, $Ncp_{trend(1880\text{-}1900)}$, $Ncp_{trend(1900\text{-}1920)}$, $Ncp_{trend(1920\text{-}1940)}$, $Ncp_{trend(1940\text{-}1960)}$, $Ncp_{trend(1960\text{-}1980)}$, $Ncp_{trend(1980\text{-}2000)}$, $Ncp_{trend(2000\text{-}2020)}$	0.610	0.574	0.568	0.592	**0.621**	0.602	0.582
$Ncp_{season(1860\text{-}1880)}$, $Ncp_{season(1880\text{-}1900)}$, $Ncp_{season(1900\text{-}1920)}$, $Ncp_{season(1920\text{-}1940)}$, $Ncp_{season(1940\text{-}1960)}$, $Ncp_{season(1960\text{-}1980)}$, $Ncp_{season(1980\text{-}2000)}$, $Ncp_{season(2000\text{-}2020)}$							
$AC_{trend(1860\text{-}1880)}$, $AC_{trend(1880\text{-}1900)}$, $AC_{trend(1900\text{-}1920)}$, $AC_{trend(1920\text{-}1940)}$, $AC_{trend(1940\text{-}1960)}$, $AC_{trend(1960\text{-}1980)}$, $AC_{trend(1980\text{-}2000)}$, $AC_{trend(2000\text{-}2020)}$							
$AC_{season(1860\text{-}1880)}$, $AC_{season(1880\text{-}1900)}$, $AC_{season(1900\text{-}1920)}$, $AC_{season(1920\text{-}1940)}$, $AC_{season(1940\text{-}1960)}$, $AC_{season(1960\text{-}1980)}$, $AC_{season(1980\text{-}2000)}$, $AC_{season(2000\text{-}2020)}$							
z, σ^2, RMSE, R^2, $PR_{ncp\text{-}mode}$, $PR_{ncp\text{-}10\%}$, $PR_{ncp\text{-}90\%}$,	0.508	0.5	0.436	0.444	0.453	0.424	0.412

Table 3
Average values of the SPI statistics for the different clusters. Colorbar ranges from red (low values) to green (high values).

	C1	C2	C3	C4	C5	C6
Min	-3.87	-3.71	-3.70	-3.84	-3.71	-4.09
Max	3.08	3.06	3.35	3.11	3.45	3.26
Mean	-0.05	0.04	0.03	-0.16	-0.12	-0.03
Median	-0.03	0.06	0.05	-0.15	-0.12	0.01
Standard Deviation	1.08	1.02	1.04	1.05	1.01	1.08
Skewness	-0.06	-0.07	-0.06	-0.04	-0.01	-0.09
Extreme drought months	75.61	50.50	55.42	85.69	64.40	76.19
Severe drought months	99.61	79.62	81.09	113.15	96.91	91.88
Moderate drought months	181.35	157.36	165.06	199.64	190.69	168.40
Near normal months	1217.27	1278.18	1257.48	1231.41	1294.69	1227.90
Moderately wet months	177.16	192.95	190.24	154.37	149.44	190.29
Severely wet months	91.42	88.11	91.54	72.14	61.73	90.08
Extremely wet months	46.45	42.52	47.98	32.55	31.72	44.63
Total number of drought months	970.41	906.60	918.33	1057.30	1041.47	944.13
Mean duration of drought events	6.05	3.87	4.59	9.25	8.19	4.79
Max duration of drought events	62.42	36.74	50.34	77.76	68.54	51.25

description of the clustering analysis, divided into clusters:

- Cluster C1 corresponded to the southwestern United Kingdom, including central and southern Wales, and southwestern England. In C1, with hilly terrain and proximity to the Irish Sea and the Atlantic Ocean, the notable topography contributes to increased precipitation. As a consequence, C1 was characterized by a relatively high number of severely and extremely wet months, second only to C3 located to the north of C1, indicating a significant humidity compared to other UK areas. All hydrological units showed a Silhouette score greater than 0.55, with the only exception being Dyfi hydrological unit, with a Silhouette score between 0.50 and 0.55. This can be justified by the proximity of Dyfi to cluster 3 in the north.
- Cluster C2 corresponded to the southeastern United Kingdom. C2, including the Thames basin with urban and agricultural regions, experiences distinct hydrological dynamics. Despite being in close proximity to water bodies, C2 exhibits the fewest drought months among all clusters, as well as the lowest mean and maximum durations of drought events. The Thames basin, a prominent

Table 4
SPI statistics for the different time scale and clusters. Colorbar ranges from red (low values) to green (high values).

	SPI-1						SPI-3						SPI-6					
	C1	C2	C3	C4	C5	C6	C1	C2	C3	C4	C5	C6	C1	C2	C3	C4	C5	C6
Min	-4.40	-4.27	-4.36	-4.41	-4.69	-4.38	-4.48	-4.07	-3.96	-3.99	-4.18	-4.20	-3.87	-4.25	-3.83	-3.91	-3.62	-4.45
Max	2.88	2.93	3.28	3.02	3.40	3.29	3.34	3.13	3.67	3.40	3.26	3.41	3.19	3.18	3.87	3.34	3.56	3.41
Mean	-0.03	0.01	0.00	-0.06	-0.05	-0.02	-0.03	0.02	0.01	-0.10	-0.07	-0.03	-0.04	0.02	0.01	-0.14	-0.10	-0.03
Median	0.05	0.08	0.07	0.02	0.02	0.07	0.00	0.06	0.03	-0.07	-0.05	-0.01	-0.01	0.06	0.03	-0.13	-0.08	0.01
Standard Deviation	1.07	1.05	1.06	1.05	1.07	1.08	1.07	1.02	1.05	1.02	1.01	1.07	1.10	1.04	1.09	1.05	1.00	1.10
Skewness	-0.23	-0.21	-0.20	-0.24	-0.20	-0.26	-0.11	-0.13	-0.08	-0.09	-0.06	-0.05	-0.08	-0.09	-0.05	-0.04	-0.05	-0.11
Extreme drought months	87.36	69.14	74.57	83.56	81.65	86.88	70.05	58.86	59.05	69.68	62.52	71.00	83.82	61.64	68.19	78.16	60.74	79.63
Severe drought months	85.86	82.86	85.57	92.32	85.78	89.00	96.86	77.57	86.76	95.64	84.65	91.38	98.59	81.57	87.57	110.36	93.09	97.25
Moderate drought months	153.05	157.79	153.86	156.64	155.22	154.13	169.95	158.07	166.19	180.80	173.26	163.75	178.77	150.93	165.48	196.48	184.91	171.13
Near normal months	1257.1	1259.5	1256.2	1284.4	1286.9	1250.6	1242.1	1286.3	1260.2	1283.9	1299.1	1250.1	1206.3	1273.4	1226.6	1240.2	1303.8	1205.1
Moderately wet months	190.82	197.00	195.33	177.80	174.30	198.00	186.59	183.64	180.38	155.24	166.87	177.13	177.82	185.07	191.10	152.60	157.09	191.00
Severely wet months	87.45	92.57	86.52	70.56	74.57	81.50	84.45	82.43	90.43	72.04	72.52	93.88	89.86	88.93	92.52	76.32	61.74	96.63
Extremely wet months	28.32	30.43	36.00	24.48	32.09	31.63	40.05	40.79	46.57	32.08	28.87	44.00	53.68	48.00	57.52	34.60	27.78	46.75
Total number of drought months	914.18	891.14	901.38	936.48	936.17	897.25	950.73	905.64	927.81	1008.32	988.35	960.75	961.27	911.14	929.24	1048.88	1018.17	946.00
Mean duration of drought events	0.93	0.92	0.90	0.99	0.98	0.89	1.90	1.75	1.78	2.18	2.05	1.73	3.06	2.76	2.78	3.98	3.57	2.68
Max duration of drought events	10.14	10.71	9.33	10.72	10.04	9.88	20.68	19.71	20.19	24.84	22.91	17.88	30.82	27.07	27.14	46.40	37.39	29.25

	SPI-12						SPI-18						SPI-24					
	C1	C2	C3	C4	C5	C6	C1	C2	C3	C4	C5	C6	C1	C2	C3	C4	C5	C6
Min	-3.58	-3.74	-3.66	-3.55	-3.27	-4.06	-3.70	-3.09	-3.40	-3.60	-3.23	-3.94	-3.19	-2.84	-2.97	-3.57	-3.26	-3.52
Max	3.16	3.26	3.42	3.13	3.51	3.35	2.97	3.01	2.96	2.92	3.52	3.09	2.92	2.88	2.92	2.87	3.46	2.99
Mean	-0.06	0.04	0.03	-0.20	-0.15	-0.03	-0.07	0.06	0.04	-0.23	-0.17	-0.03	-0.07	0.06	0.06	-0.24	-0.19	-0.02
Median	-0.05	0.05	0.04	-0.21	-0.16	-0.01	-0.07	0.07	0.04	-0.24	-0.20	-0.01	-0.09	0.04	0.06	-0.26	-0.23	0.01
Standard Deviation	1.10	1.02	1.06	1.06	0.99	1.09	1.08	0.99	1.01	1.06	1.00	1.08	1.06	0.96	0.97	1.06	1.02	1.06
Skewness	-0.01	-0.02	-0.01	0.04	0.06	-0.04	0.02	-0.03	0.00	0.05	0.08	-0.04	0.04	0.06	-0.02	0.05	0.12	-0.08
Extreme drought months	78.18	46.86	54.71	90.88	56.30	76.13	72.68	38.14	41.38	94.32	62.26	72.88	61.59	28.36	34.62	97.52	62.91	70.63
Severe drought months	104.59	78.50	79.14	119.12	100.17	84.13	103.23	77.71	77.52	128.48	106.00	90.75	108.50	79.50	69.95	133.00	111.78	98.75
Moderate drought months	188.86	162.64	172.19	209.76	198.52	174.25	196.36	161.64	169.00	226.20	207.78	178.88	201.09	153.07	163.67	227.96	224.43	168.25
Near normal months	1192.6	1271.2	1234.8	1209.6	1310.5	1216.3	1195.0	1273.6	1266.4	1188.0	1293.2	1211.6	1210.5	1305.1	1300.7	1182.2	1274.6	1233.6
Moderately wet months	170.77	188.50	194.14	148.12	139.65	192.00	171.86	207.93	192.81	149.72	132.30	196.88	165.09	195.57	187.67	142.72	126.43	186.75
Severely wet months	95.73	91.71	99.05	75.52	55.35	95.88	98.50	87.64	91.43	68.28	54.91	90.38	92.55	85.36	89.29	70.12	51.30	82.25
Extremely wet months	56.64	49.57	56.19	35.24	30.65	50.13	50.86	43.07	48.86	34.60	33.43	47.88	49.18	43.29	42.71	34.28	37.48	47.38
Total number of drought months	986.64	914.00	927.90	1103.88	1087.26	959.13	997.77	903.14	918.29	1118.28	1103.13	959.38	1011.86	914.50	905.33	1127.96	1115.74	942.25
Mean duration of drought events	6.25	4.65	5.44	9.99	8.24	5.48	9.80	6.05	7.14	14.93	13.59	7.22	14.36	7.07	9.51	23.47	20.69	10.74
Max duration of drought events	65.00	44.00	59.00	90.20	71.83	59.50	103.36	55.00	77.33	126.24	116.35	73.50	144.55	63.93	109.05	168.16	152.70	117.50

feature in this cluster, significantly influences local hydrology, reflecting how specific geographic features can mitigate drought conditions. Similar to C1, C2 also exhibited Silhouette scores greater than 0.50, indicating a relevant belonging of the hydrological units to the cluster.

- Cluster C3 covers the West and East England Midlands and the North of Wales, exhibiting a Silhouette score ranging between 0.50 and 0.70. C3 is distinguished by a higher frequency of severely and extremely wet months, surpassing the total number of drought months observed in C2. Notably, C3 incorporates the Isle of Man, situated in the Irish Sea between England and Northern Ireland. The Isle exhibits a distinctive pattern, potentially influenced by its geographical location, with a Silhouette score ranging from 0.45 to 0.50, indicating a comparatively lower affiliation with C3. It is important to note that geographical factors contribute to variations. While the Isle of Man is located in the Irish Sea, potentially moderating its climate, the UK mainland experiences a range of climates influenced by its diverse topography and proximity to large water bodies. Interestingly, despite the moderate climatic distinctions, the Isle of Man demonstrates drought features more akin to Cluster C3, especially concerning abrupt changes in trends. This suggests that, although geographical location does play a role in shaping climatic patterns, there are other influencing factors contributing to the Isle of Man aligning more closely with Cluster C3 than with other clusters. This could be attributed to specific local or regional factors that exert a stronger influence on the Isle of Man's climate, creating a unique dynamic within the broader context of the UK clusters.
- Cluster C4 corresponded to southern Scotland, including significant hydrological units such as Tweed and Tay. C4 was characterized by a varied topography with mountains and valleys, contributing to the highest number of drought months, including severe and extreme droughts months, as well as the longest mean and maximum durations of drought events. The hydrological units showed also a quite good belonging to cluster, with Silhouette scores between 0.50 and 0.65.
- Cluster C5 included northern Scotland, starting from hydrological units like Spey and Dee. C5 is characterized by the presence of mountain ranges that contribute to unique climatic conditions and hydrological patterns. Silhouette scores were between 0.50 and 0.65, except for the Lochy (Invernesshire) hydrological unit which, however, was at the border with C4. Additionally, it exhibited features similar to C4, with, however, a lower number of months characterized by drought events, especially extreme ones.
- Cluster C6 corresponded to the Northern Ireland territory. Cluster C6 features diverse landscapes, including coastal areas and inland waters. The proximity to the North Channel and the Irish Sea can influence the local climate and hydrological characteristics. In particular, the hilly topography contributes to variations in precipitation and runoff. The elevation changes within the cluster may also influence the distribution of water resources and weather patterns. It showed very high Silhouette Scores, between 0.65 and 0.7. C6 hydrological units demonstrate a strong belonging to the cluster while, at the same time, showing a marked difference from the rest of the investigated territory. C6 exhibited the lowest SPI values overall, with, however, a slightly higher number of drought months compared to cluster C3. Nevertheless, compared to the latter, the number of months characterized by extreme drought is significantly higher, with values lower than the only cluster C4.

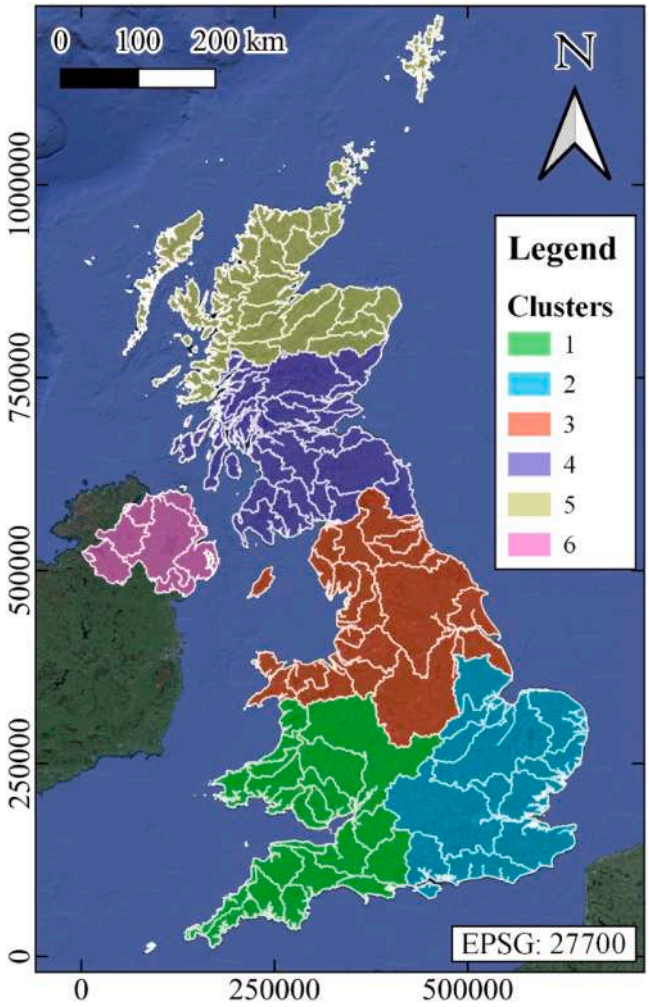

Fig. 2. SPI clustering of UK. White lines indicate the different hydrological units falling within each cluster.

It must be pointed out the role of the Silhouette scores in interpreting each cluster's characteristics, providing insights into the internal cohesion and homogeneity of weather patterns within the clusters. A higher Silhouette score indicates a more well-defined and internally consistent cluster, suggesting a greater similarity in meteorological features among its hydrological units. For instance, C6 with a notably high mean Silhouette score of 0.69, and a low standard deviation of the Silhouette score of 0.02, reflects strong internal similarity among its hydrological units, emphasizing a distinct and consistent meteorological profile. Correlating Silhouette scores with observed weather patterns involves understanding the degree of similarity among hydrological units within a cluster. In the context of the provided clusters, the scores signify the degree of alignment in climatic conditions. For instance, C4, characterized by a varied topography in southern Scotland, exhibits a mean Silhouette score of 0.61, indicating notable internal cohesion. This suggests that hydrological units within C4 share more similar weather patterns, which, when further examined with SPI values, could imply a consistent prevalence of drought (or humidity) conditions, aligning with the topographical influences on climatic characteristics.

3.2. Seasonal MK analysis

The monthly distribution of Z and β for SPI at various time scales and across each cluster is illustrated in Fig. 4. Furthermore, the p-values obtained through the seasonal MK test are marked on each plot. These p-values serve as indicators to evaluate clusters with noteworthy trends. Earlier research on hydrological trends conventionally adopted a significance threshold of p (where trends are considered significant) at 0.01 (Shahfahad et al., 2023). Moreover, the values of Z, β and p, with the test for statistically significant trend ($p \leq 0.01$), are given in Table 5.

Positive values of both Z and β were computed for all clusters, with the exception of the south-eastern cluster C2, which instead showed negative values of both Z and β. From SPI-1 to SPI-24, an increase in both Z and β was observed, indicating more pronounced trends as the SPI time scale increases. Specifically, significant increasing trends were observed in cluster C4 (southern Scotland), with a Z that ranges between 4.124 for SPI-1 and 20.229 for SPI-24. Overall, the clusters located further north exhibited more pronounced

Fig. 3. Silhouette scores for the six clusters.

increasing trends, with C5 (northern Scotland, Z ranging between 2.385 for SPI-1 and 9.908 for SPI-24) and C6 (Northern Ireland, Z ranging between 2.397 for SPI-1 and 13.126 for SPI-24) being characterized by higher Z and B values compared to C1 (south-west England, Z ranging between 1.883 for SPI-1 and 8.491 for SPI-24) and C3 (northern England, Z ranging between 0.845 for SPI-1 and 6.705 for SPI-24).

In addition, C4 was the only cluster that showed statistically significant trends for all SPI time scales. However, from SPI-6 to SPI-24, all clusters with the exception of C2, showed statistically significant trends. For SPI-3, in addition to C2, C3 showed a p-value higher than 0.044, greater than 0.01, yet still relatively small and below 0.05. Therefore, although C2 exhibited decreasing trends across all time scales, these are not statistically significant.

The singularity of Cluster C2 can be attributed to the unique aspects of south-eastern England. Specifically, this area is characterized by significantly lower average precipitation compared to the rest of the United Kingdom, particularly when compared to the western coast. Indeed, the disparities between the western and eastern regions of the UK can be explained by the UK's rainfall patterns, with the topography favoring more rainfall on the west coast than on the east coast. However, despite the rainfall patterns, as discussed in Section 3.1, C2 showed the fewest drought months among all clusters, with the lowest mean and maximum durations of drought events. Hence, these factors can be associated with the slightly negative SPI trends, though not statistically significant, observed in the southeast of the UK.

On the contrary, clusters like C4, which exhibited a high number of dry months, display increasing trends in SPI across various temporal scales, indicating a climate that is becoming wetter.

3.3. BEAST analysis

The first aspect addressed through the BEAST analysis involves the assessment of changepoints in the trends. Table 6 provides for each cluster and SPI, the mean number of changepoints in trend. As the number of hydrological units varies from cluster to cluster, the value presented in the table represents the average calculated among the hydrological units within each cluster. Overall, the twenty-

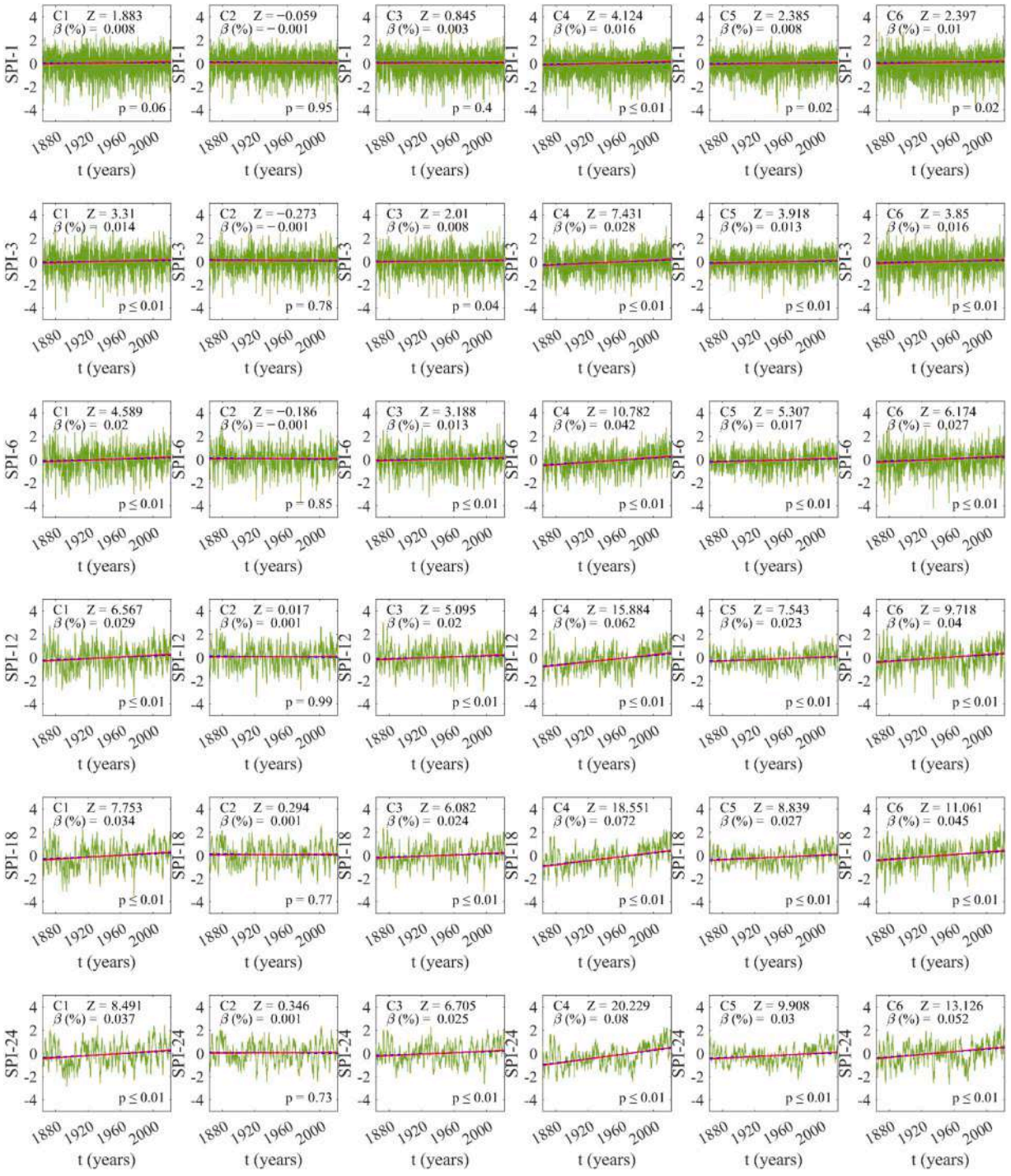

Fig. 4. Distribution of Z and β for SPI at the different time scale. The red line indicates the median slope while the blue and magenta dashed lines indicate the confidence intervals. Output obtained by the software MATLAB (The MathWorks Inc. Optimization Toolbox version: 9.0.13 R2022b).

year period that exhibited the highest mean number of changepoints in trend was 1860–1880 (mean value of 1.67 computed on all clusters and SPI time scales), followed by the period 1980–2000 (mean value of 1.61). On the other hand, the twenty-year period that exhibited the lowest mean number of changepoints in trend was 1900–1920 (mean value of 0.69), followed by 1900–1920 (mean value of 0.69). In addition, higher SPI scales (e.g., 18 and 24 months) showed more changepoints in trend compared to the lower SPI scales (e.g., 1 and 3 months), within the same cluster. Moreover, Table 7 provides the mean trend abrupt change for each cluster and SPI scale. SPI-1 exhibited very limited instances of abrupt change, ranging between −4.26% (C5, 1860–1880), indicating a quite negative

Table 5
Seasonal MK parameters computed for the SPI at the different time scales, for each cluster. For Z and β, colorbar ranges from red (low values) to green (high values). For the p-values, colorbar ranges from green (low values) to red (high values). In addition, the test for statistically significant trend ($p \leq 0.01$) is reported.

SPI time scales	MK parameters	Clusters					
		C1	C2	C3	C4	C5	C6
SPI-1	Z	1.883	-0.059	0.845	4.124	2.385	2.397
	β (%)	0.008	0.001	0.003	0.016	0.008	0.010
	p-value	0.060	0.953	0.398	< 0.10	0.017	0.017
	Stat.sign.	No	No	No	Yes	No	No
SPI-3	Z	3.310	-0.273	2.010	7.431	3.918	3.850
	β (%)	0.014	-0.001	0.008	0.028	0.013	0.016
	p-value	0.001	0.785	0.044	< 0.10	0.000	0.000
	Stat.sign.	Yes	No	No	Yes	Yes	Yes
SPI-6	Z	4.589	-0.186	3.188	10.782	5.307	6.174
	β (%)	0.020	-0.001	0.013	0.042	0.017	0.027
	p-value	< 0.10	0.852	< 0.10	< 0.10	< 0.10	< 0.10
	Stat.sign.	Yes	No	Yes	Yes	Yes	Yes
SPI-12	Z	6.567	0.017	5.095	15.884	7.543	9.718
	β (%)	0.029	0.001	0.020	0.062	0.023	0.040
	p-value	< 0.10	0.986	< 0.10	< 0.10	< 0.10	< 0.10
	Stat.sign.	Yes	No	Yes	Yes	Yes	Yes
SPI-18	Z	7.753	0.294	6.082	18.551	8.839	11.061
	β (%)	0.034	0.001	0.024	0.072	0.027	0.045
	p-value	< 0.10	0.769	< 0.10	< 0.10	< 0.10	< 0.10
	Stat.sign.	Yes	No	Yes	Yes	Yes	Yes
SPI-24	Z	8.491	0.346	6.705	20.229	9.908	13.126
	β (%)	0.037	0.001	0.025	0.080	0.030	0.052
	p-value	< 0.10	0.729	< 0.10	< 0.10	< 0.10	< 0.10
	Stat.sign.	Yes	No	Yes	Yes	Yes	Yes

change in trend, and 0.53% (C5, 1900–1920), indicating a modest positive change in trend.

Transitioning to SPI-3, more pronounced abrupt changes were observed. In particular, values between −6.38% (C2, 1860–1880), and 16.61% (C2, 1960–1980), were computed. From this perspective, the BEAST analysis representation for the Norfolk hydrological unit (SPI-3, C2) is given in Fig. 5a. The latter highlighted negative trends for the periods between 1875 and 1910 (the blue color indicates the probability of the trend slope is negative), and also after 2000. At the same time, no relevant changepoints in trends were observed in the period between 1910 and 2000 (green color indicates the probability of no relevant trend). This result was in agreement with what was observed with the MK test, which showed slightly decreasing SPI trends for C2. However, discrepancies were also observed in relation to the MK test, with decades such as 1960–1980 showing a marked positive trend abrupt change across the entire C2 (16.61%).

For time scales ranging from 6 to 24 months, significant trend abrupt changes can be observed across various two-decade intervals and different clusters. Values range from −51.10% (C5, SPI-18, 1860–1880) to 34.50% (C6, SPI-24, 1860–1880) in total. In particular, the output of the BEAST analysis for the Conon hydrological unit (C5), at a time scale of 18 months was represented in Fig. 5b, showing a particularly negative trend in the period 1860–1880, in agreement with the rest of C5, with positive trends (red color indicates the probability of trend slope being positive) between 1920 and 1980. Moreover, Fig. 5c provides the output of the BEAST analysis for the Loughor hydrological unit, included in C1, at a time scale of 24 months, which showed marked positive trends in the last 20 years and also during the 1895–1910 period. Here too, there are clear differences between the BEAST analysis and the seasonal MK test. BEAST was capable of identifying periods marked by abrupt reductions in SPI, transitioning from humid to drought conditions, which the MK test fails to capture. It must be point out that the marked positive trends that was observed in Southwest England in the last decade aligns with the winter 2013–2014 storms. In particular, in late 2013 and early 2014, brought heavy rainfall and widespread flooding to parts of the UK, including the southern England where the cluster C1 is located. The floods had significant economic and social impacts.

Furthermore, it has been observed that, within the same decades, the clusters exhibited significant differences. For example, in the periods 1860–1880 and 1880–1900, C1 and C2, in the south of England, showed marked positive mean trend abrupt change at intermediate SPI time scales, while C5 and C6, in the north of England, highlighted marked negative mean trend abrupt change for the same SPI time scales. Even among the most recent twenty-year periods, from 1980–2000 and 2000–2020, substantial differences were evident within the clusters. Specifically, the distinct and noticeable positive abrupt changes in trend observed within C1, C2, and C3 in the southern and central regions of the United Kingdom during the 1980–2000 timeframe were not apparent within the other clusters, corresponding to Scotland and Northern Ireland. Simultaneously, in the most recent twenty-year period, C4 (southern Scotland) and C6 (Northern Ireland) exhibited prominent negative abrupt changes in trend that were absent in the remaining clusters, except for C2

Table 6
Mean number of changepoints in trend for each cluster and SPI scale. Colorbar ranges from red (low values) to green (high values).

Cl.	SPI scale	Mean number of changepoints in trend							
		1860-1880	1880-1900	1900-1920	1920-1940	1940-1960	1960-1980	1980-2000	2000-2020
1	1	1.41	1.41	2.27	1.50	0.82	0.68	0.91	0.64
	3	1.77	1.18	1.27	1.27	0.23	1.45	1.32	0.95
	6	2.09	0.95	1.45	1.64	0.18	1.09	1.23	1.00
	12	1.00	1.41	1.50	1.50	0.41	1.82	0.95	1.36
	18	1.09	1.55	1.18	1.59	0.77	1.41	1.23	1.18
	24	1.14	1.32	1.23	1.45	0.59	1.59	1.32	1.32
2	1	1.40	1.67	0.53	0.93	1.00	1.00	1.53	1.60
	3	1.53	0.60	0.93	1.87	0.07	1.13	2.07	1.20
	6	1.80	0.87	0.73	1.40	0.27	0.73	2.33	1.60
	12	1.67	0.93	1.00	2.13	0.40	1.13	1.67	1.07
	18	1.40	1.33	1.13	1.60	0.47	0.93	1.87	1.27
	24	1.07	0.93	0.87	2.00	0.60	1.27	2.20	1.07
3	1	0.90	1.05	1.00	1.20	1.05	0.90	2.00	1.00
	3	1.65	1.25	0.25	2.00	0.40	1.35	2.45	0.30
	6	1.40	1.60	0.30	1.65	0.40	1.65	2.30	0.45
	12	1.15	1.25	0.65	1.35	0.65	1.90	1.90	1.10
	18	1.25	1.25	0.70	1.35	0.65	1.95	1.95	0.90
	24	0.90	1.35	0.55	1.35	0.70	1.85	2.20	1.10
4	1	0.92	1.12	0.04	0.12	0.23	1.50	5.19	0.15
	3	3.27	1.62	0.62	0.54	0.69	1.35	0.88	0.50
	6	2.50	1.69	0.62	0.54	0.88	1.23	1.12	0.85
	12	1.81	1.12	0.62	0.92	0.92	1.69	0.88	1.69
	18	1.92	1.42	0.69	0.77	1.19	1.31	1.50	1.04
	24	1.81	1.46	0.46	0.92	1.38	1.38	1.38	1.15
5	1	1.23	1.27	1.59	0.41	0.77	0.82	3.14	0.45
	3	2.14	1.05	1.00	0.68	0.59	1.55	1.41	1.59
	6	1.86	1.27	0.91	0.36	0.73	1.45	1.50	1.82
	12	2.14	1.14	1.05	0.41	0.86	1.50	1.64	1.27
	18	2.14	1.23	1.09	0.36	1.18	1.45	1.27	1.27
	24	1.73	1.41	1.00	0.45	1.00	1.55	1.41	1.45
6	1	1.88	2.75	0.13	0.50	0.13	0.50	3.00	0.75
	3	3.00	2.25	0.50	1.88	0.75	1.00	0.13	0.38
	6	2.38	1.88	0.50	1.38	0.50	1.75	0.25	1.25
	12	2.00	1.25	0.63	1.25	0.75	1.63	0.50	1.88
	18	1.13	1.25	0.88	0.88	1.38	1.88	0.75	1.50
	24	1.50	1.50	1.13	1.50	1.25	1.88	0.50	0.75

in the case of SPI-24. In this respect, mention can be made of the summer of 2018, which saw a prolonged heat wave accompanied by below-average rainfall, with parts of Northern Ireland and Scotland experiencing drier than average conditions.

The second aspect investigated through the BEAST analysis involves the assessment of changepoints in seasonality. It is important to highlight that, while both trends and seasonality play a role in shaping the overall behavior of time series data, the distinction

Table 7
Mean trend abrupt change for each cluster and SPI scale. Colorbar ranges from red (low values) to blue (high values).

Cl.	SPI scale	Mean trend abrupt change (%)							
		1860-1880	1880-1900	1900-1920	1920-1940	1940-1960	1960-1980	1980-2000	2000-2020
1	1	-0.07	-0.05	0.04	0.00	0.00	0.00	0.00	0.00
	3	-0.41	-4.32	4.24	-2.87	-0.46	9.63	4.69	-2.92
	6	2.30	-13.73	10.21	-6.87	-2.61	13.32	11.36	-1.28
	12	17.71	-15.91	7.06	0.61	0.58	12.68	12.78	0.44
	18	13.94	-17.33	21.43	-7.55	3.34	-6.80	22.66	4.69
	24	7.14	-30.53	6.03	2.05	7.97	-13.49	25.59	1.45
2	1	0.00	0.00	0.00	0.00	0.00	0.00	0.00	0.00
	3	7.22	-6.38	3.04	0.10	0.26	16.61	6.76	-0.27
	6	20.04	-16.22	13.25	-2.67	2.14	12.33	-3.12	8.36
	12	29.81	-22.52	18.73	-3.07	-1.54	4.65	7.46	0.11
	18	8.95	-38.03	13.37	5.89	2.83	2.28	8.87	0.07
	24	3.54	-31.15	6.66	13.28	2.12	-3.08	12.45	-17.57
3	1	0.00	-0.01	0.00	0.00	0.00	0.00	0.01	0.00
	3	5.32	-7.37	2.49	-1.21	-0.27	1.98	-1.48	0.78
	6	0.55	-18.90	0.21	-8.81	2.53	5.81	-2.95	3.83
	12	-7.16	-31.45	-8.95	-2.64	-3.32	4.16	5.26	3.40
	18	-4.80	-30.32	-2.93	-10.01	-1.30	13.20	10.28	7.08
	24	-0.57	-34.76	-7.59	-28.84	-0.62	4.48	14.02	-6.30
4	1	-0.03	-0.01	0.01	-0.01	0.00	0.11	0.17	0.00
	3	-1.17	5.67	1.11	-0.98	0.76	2.16	1.54	0.49
	6	-9.08	5.96	0.55	-5.16	1.50	4.80	0.94	-1.20
	12	-38.76	1.53	-2.06	-15.13	-8.49	4.36	-6.71	-25.40
	18	-12.64	9.48	-1.53	-4.56	-0.98	-12.16	-3.31	-7.35
	24	-16.23	1.60	0.29	-5.34	4.67	-6.18	-8.08	-21.64
5	1	-4.26	0.00	0.53	0.00	0.04	0.04	0.06	-0.01
	3	-4.05	3.48	-1.87	-0.24	4.44	1.44	-1.20	-1.81
	6	-12.54	11.29	-1.11	-2.23	5.22	1.44	1.27	-5.56
	12	-12.27	12.70	3.59	-5.27	10.81	-1.93	-0.26	-6.72
	18	-51.10	9.04	1.95	-0.21	14.35	-5.29	-3.05	4.02
	24	-22.22	22.88	0.24	1.19	17.85	10.71	2.55	8.85
6	1	0.00	0.04	0.01	0.00	0.00	0.00	0.02	0.00
	3	2.53	2.54	-0.39	1.48	-1.92	1.25	0.37	-1.37
	6	-0.44	-0.27	-0.66	1.12	-3.26	3.93	-2.25	-1.88
	12	4.16	-4.07	2.90	-18.82	-4.47	2.77	0.11	-8.98
	18	-31.14	-2.82	7.01	-3.32	12.45	11.04	0.05	-26.01
	24	34.50	1.29	-15.41	-19.97	-17.70	20.35	1.69	-11.34

between them lies in their time scales and the nature of their variations. In particular, while trends can be defined as long-term movements that describe the general direction of the data over an extended period, seasonality represents the regular and predictable pattern of fluctuations that repeat within shorter time intervals. Therefore, an increase in the seasonality of drought events results in a higher frequency or severity of drought periods during specific seasons of the year. This means that dry seasons become more

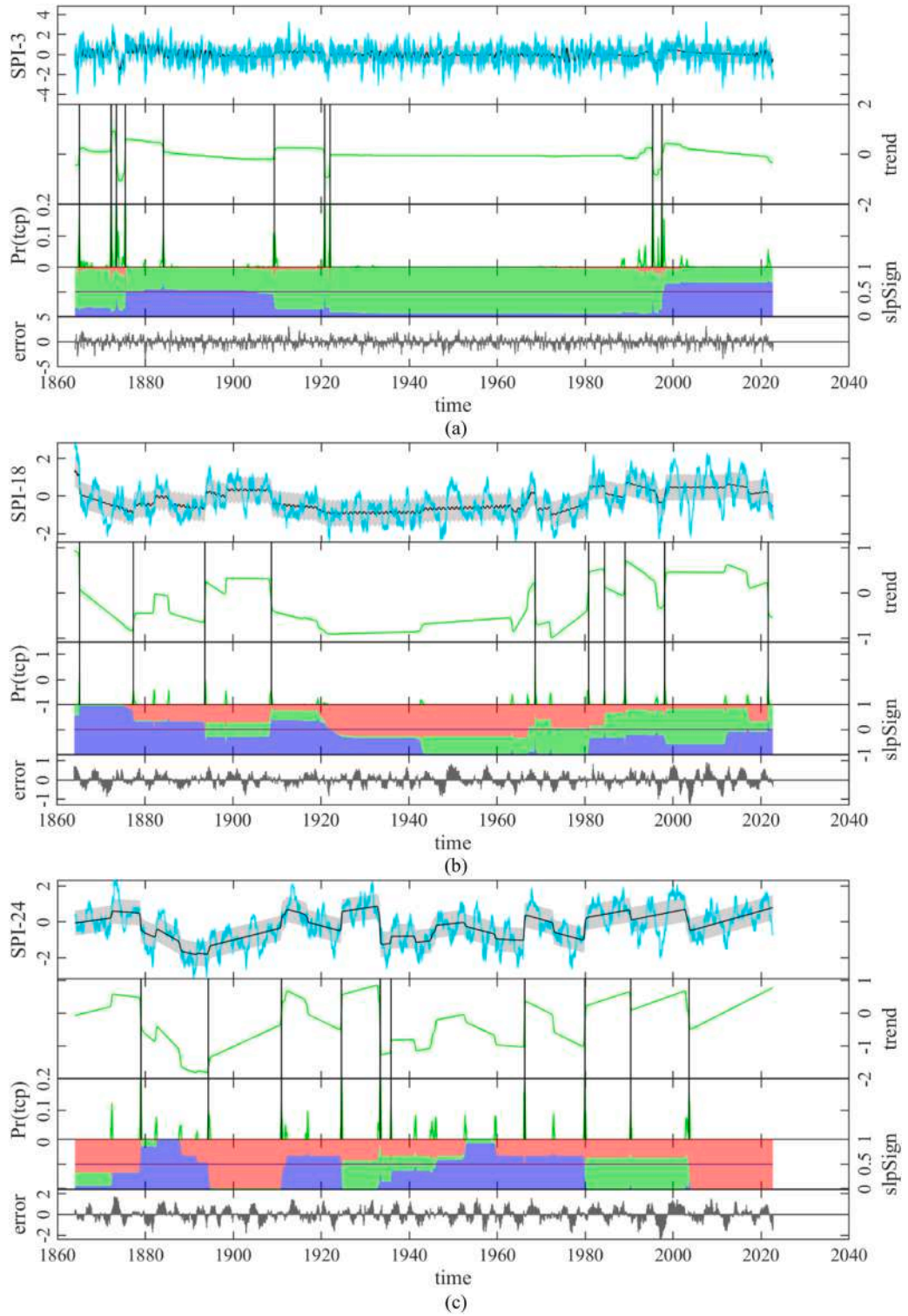

Fig. 5. Trend analysis for: Norfolk hydrological unit – SPI-3 – C2 (a); Conon hydrological unit – SPI-18 – C5 (b); Loughor hydrological unit – SPI-24 – C1 (c). Pr(tcp) indicates the probability of trend changepoint.

prolonged or severe, with potentially significant consequences for agriculture, water resources, ecosystems, and the availability of drinking water.

Table 8 provides for each cluster and SPI, the mean number of changepoints in seasonality. Overall, the twenty-year period that

Table 8
Mean number of changepoints in seasonality for each cluster and SPI scale. Colorbar ranges from red (low values) to green (high values).

Cl.	SPI scale	Mean number of changepoints in seasonality							
		1860-1880	1880-1900	1900-1920	1920-1940	1940-1960	1960-1980	1980-2000	2000-2020
1	1	1.82	0.55	0.00	0.05	0.45	7.05	0.00	0.09
	3	1.18	2.00	0.82	1.45	0.73	1.64	0.23	1.95
	6	1.09	1.86	1.05	1.45	0.14	1.55	0.50	2.36
	12	1.50	1.23	0.82	1.91	1.00	1.45	0.73	1.27
	18	1.41	0.73	0.68	0.55	0.27	4.27	0.55	1.23
	24	1.36	0.45	0.91	1.77	1.14	1.32	0.86	2.09
2	1	1.73	0.07	0.33	0.33	0.13	4.27	2.27	0.67
	3	1.33	2.47	0.27	1.20	0.67	2.67	0.80	0.60
	6	1.07	2.67	0.40	0.93	0.73	2.67	0.80	0.73
	12	1.47	0.33	1.20	1.47	1.87	2.00	0.53	0.93
	18	1.80	0.13	0.93	1.40	0.53	2.53	1.27	1.00
	24	1.67	0.33	0.53	1.47	1.53	1.27	1.67	1.40
3	1	1.35	0.05	0.10	0.55	0.70	6.05	0.50	0.35
	3	1.55	0.85	0.50	0.50	1.70	2.20	0.20	2.50
	6	1.50	1.00	0.80	1.10	1.30	1.25	0.80	2.25
	12	1.35	0.90	1.30	1.75	1.80	0.60	0.70	1.45
	18	2.95	0.55	1.40	1.05	0.35	1.65	0.70	0.85
	24	2.25	1.00	0.90	1.25	1.40	1.00	1.00	0.95
4	1	0.23	0.04	0.00	0.19	0.08	6.85	2.08	0.31
	3	0.96	0.15	2.12	0.62	0.12	2.23	1.81	2.00
	6	1.62	0.69	2.15	0.46	0.08	1.58	1.04	2.35
	12	1.23	0.92	1.15	1.35	2.15	0.42	0.77	1.81
	18	2.35	0.65	1.23	0.65	0.50	1.62	1.19	1.50
	24	2.35	1.54	1.42	0.42	1.42	0.62	0.65	1.23
5	1	1.18	0.23	0.36	0.32	0.05	6.32	1.41	0.14
	3	1.36	0.77	1.77	1.86	0.09	1.91	2.00	0.23
	6	1.59	1.00	1.59	1.73	0.05	1.86	1.50	0.68
	12	1.45	1.14	0.64	1.27	0.82	1.59	0.91	2.14
	18	2.77	0.50	0.91	0.77	0.41	2.27	0.95	1.41
	24	2.18	0.45	1.36	0.91	1.45	1.14	0.95	1.50
6	1	1.13	0.00	0.00	0.13	0.13	8.63	0.00	0.00
	3	2.25	1.88	1.38	0.13	0.13	1.00	1.50	1.75
	6	2.75	2.25	1.38	1.00	0.00	0.88	0.75	1.00
	12	1.75	2.00	0.63	1.63	2.13	0.38	0.25	1.13
	18	4.38	2.63	0.50	1.25	0.25	0.75	0.13	0.00
	24	2.25	1.88	0.25	1.63	1.25	0.38	1.00	1.25

exhibits the highest mean number of changepoints in seasonality was 1860–1880 (mean value of 2.39 computed on all clusters and SPI time scales), while the twenty-year period that exhibits the lowest mean number of changepoints in trend was 1940–1960 (mean value of 0.77). Furthermore, unlike trends, for the seasonality, there isn't an increase in the average number of changepoints as the SPI monthly scale increases. The mean number of changepoints in seasonality is consistently higher for temporal scales of 3 and 6 months.

Table 9 provides the mean season abrupt change for each cluster and SPI scale. In contrast to the trends, in the case of seasonality, it is the SPI-24 that showed the smallest values of season abrupt change. SPI-1 exhibited season abrupt change between −1.86% (C5, 1880–1900), indicating a modest negative seasonal change, and 10.33% (C5, 1900–1920), indicating a quite positive seasonal change. Transitioning to SPI-3, greater seasonal abrupt changes can be observed, ranging between −19.69% (C6, 1880–1900), and 16.61%

Table 9
Mean season abrupt change for each cluster and SPI scale. Colorbar ranges from red (low values) to blue (high values).

Cl.	SPI scale	Mean season abrupt change (%)							
		1860-1880	1880-1900	1900-1920	1920-1940	1940-1960	1960-1980	1980-2000	2000-2020
1	1	0.96	-0.52	0.00	0.48	-0.15	-0.74	0.00	0.30
	3	7.33	1.56	0.68	-4.59	-1.76	-2.66	-0.47	4.64
	6	2.03	13.66	-3.07	-9.30	-0.07	-7.34	-1.43	-2.34
	12	0.00	-0.01	-0.01	0.00	-0.01	0.00	0.00	0.00
	18	0.96	-0.34	-0.68	0.69	0.10	-0.81	-0.12	-0.03
	24	0.00	0.00	-0.01	-0.01	0.00	0.00	0.00	0.00
2	1	0.35	-0.02	-0.01	-0.12	-0.03	-0.09	0.91	-0.25
	3	7.21	-3.33	0.60	0.05	-1.18	-4.58	1.25	3.98
	6	24.75	4.47	-1.47	-5.22	-3.46	-13.52	2.28	0.84
	12	0.00	0.00	0.01	0.00	-0.01	0.00	0.00	0.00
	18	0.45	0.00	-0.29	-0.80	-0.11	0.08	0.10	-0.05
	24	0.00	0.00	0.01	0.00	0.00	0.00	0.00	0.00
3	1	0.67	0.00	-0.35	-0.60	0.09	0.26	0.14	0.71
	3	-5.28	3.00	0.51	3.13	-6.72	-3.45	-0.24	0.24
	6	-1.08	5.53	-1.18	0.30	-3.97	-4.19	3.61	1.88
	12	0.00	-0.01	0.00	0.00	-0.01	0.00	0.00	0.00
	18	2.06	-0.16	0.42	-0.76	-0.02	0.17	0.14	0.19
	24	0.00	0.00	0.00	0.00	0.00	0.00	0.00	0.00
4	1	0.46	0.04	0.00	-0.21	0.12	1.78	0.28	0.00
	3	-5.49	0.72	0.28	5.86	-0.66	4.88	-7.13	1.77
	6	6.34	-0.91	-1.38	3.08	0.09	2.88	2.61	-0.68
	12	-0.73	0.01	0.00	-0.01	-0.01	0.00	0.00	-0.01
	18	-0.03	-0.66	0.06	0.43	0.03	-0.05	0.24	0.01
	24	0.00	-0.01	-0.01	0.00	-0.01	0.00	0.00	0.01
5	1	7.74	-1.86	0.14	0.17	-0.01	-0.07	0.33	0.03
	3	-4.39	5.70	9.52	0.26	-1.64	-6.68	-7.98	1.18
	6	-0.67	0.22	-1.25	-0.21	0.19	-1.84	3.20	1.60
	12	-4.12	0.00	-0.01	0.00	0.00	0.01	0.00	0.00
	18	0.37	0.47	0.32	0.36	0.02	-2.79	1.51	0.32
	24	0.00	0.01	-0.01	-0.01	0.00	-0.01	0.00	0.00
6	1	10.33	0.00	0.00	0.28	-1.32	1.16	0.00	0.00
	3	16.47	-19.69	-9.88	2.42	3.73	1.36	1.39	-2.24
	6	-5.40	0.91	3.34	3.77	0.00	1.38	5.19	-2.13
	12	0.00	0.00	0.01	0.00	-0.01	0.00	-0.01	0.01
	18	-6.89	8.20	-0.53	1.81	-3.10	0.53	0.11	0.00
	24	0.00	0.00	0.00	0.00	0.01	0.00	-0.01	-0.01

(C6, 1860–1880). For C6 and SPI-3, the output of the BEAST analysis for the Foyle hydrological unit is given in Fig. 6a. For the latter, no significant trends were observed. However, considerable variations in seasonality can be appreciated, with significant abrupt changes, both positive and negative, throughout the entire time series. Relevant abrupt changes can also be observed for SPI-6. Fig. 6b

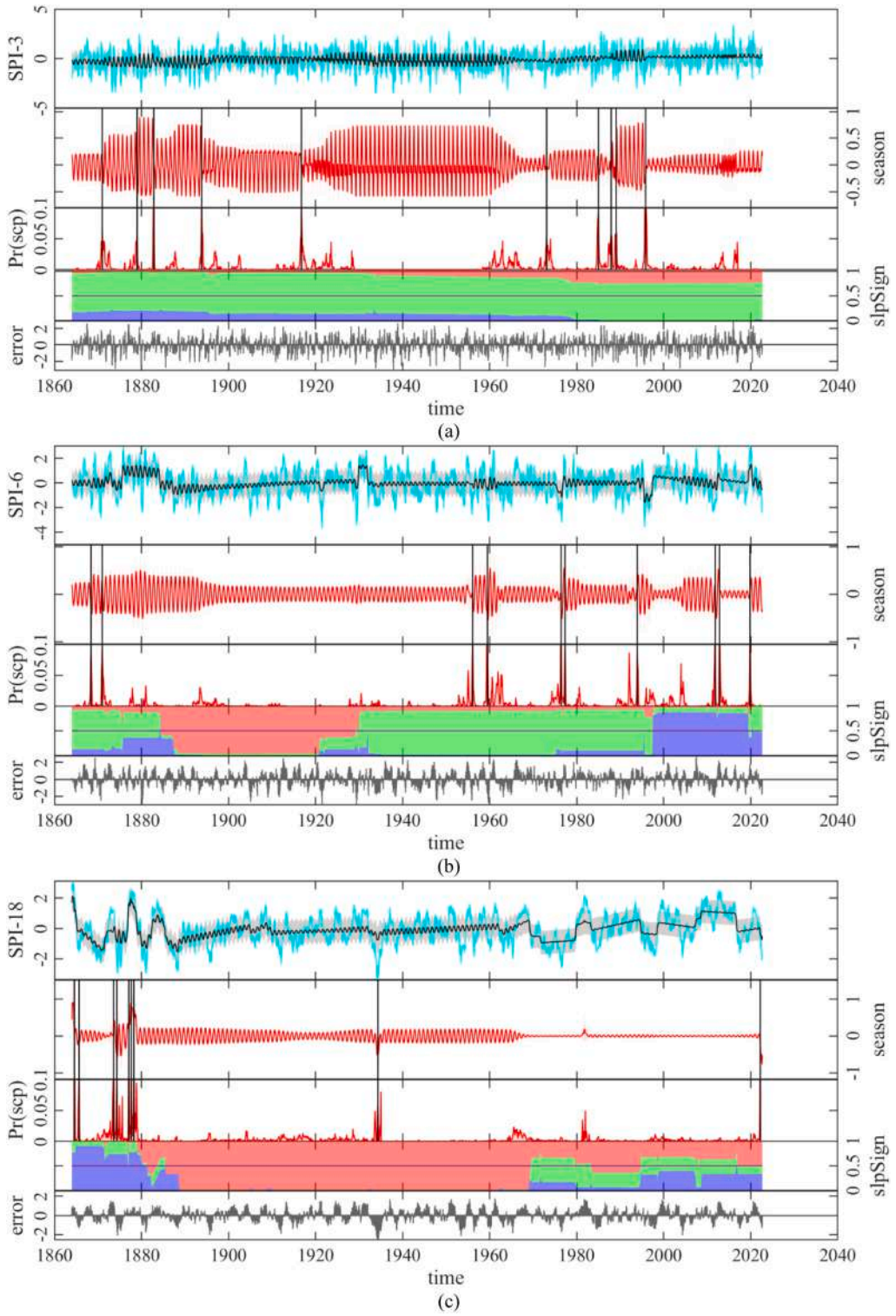

Fig. 6. Season analysis for: Foyle hydrological unit – SPI-3 – C6 (a); Trent hydrological unit – SPI-6 – C3 (b); Bush hydrological unit – SPI-18 – C6 (c). Pr(scp) indicates the probability of season changepoint.

provides, for SPI-6, the BEAST analysis for the Trent hydrological unit, included in C3. In particular, abrupt changes can be observed from 1960 up to the present day, encompassing both positive and negative changes. Additionally, it is noteworthy that abrupt seasonal changes did not exhibit a significant correlation with abrupt changes in trends. The latter trend changes, in particular, showed a tendency to be negative throughout the period from 2000 to 2020.

Time scales ranging from 12 to 18 months showed less relevant seasonal abrupt changes. However, Fig. 6c provides, for SPI-18, the BEAST analysis for the Bush hydrological unit, included in C6. The latter exhibited predominantly concentrated seasonal abrupt changes between 1860 and 1900, which appear to be correlated with the negative trend abrupt changes evident in the same period.

The positive or negative variations in seasonality identified in this study would have far-reaching implications for the present case study. An increase in the seasonality of drought events, particularly observed in temporal scales of 3 and 6 months, would lead to a higher frequency and severity of drought periods during specific seasons. This intensification of dry seasons would have potential threats to agriculture, water resources, ecosystems, and the availability of drinking water. Overall, the significant abrupt changes in seasonality, both positive and negative, highlighted by the BEAST analysis, would offer valuable insights into the dynamic nature of drought patterns, crucial for informed decision-making and adaptive strategies.

A combined box and violin plots representation (Legouhy, 2023) of trend and seasonal abrupt changes is given in Figs. 7 and 8, respectively. Regarding trend abrupt changes, the median values were close to 0 for SPI-1, while they took on greater values for the higher temporal scales. For SPI-18, C1, C2 and C5 showed positive median values (to which corresponds a greater tendency for positive trend abrupt changes), while C3, C4 and C6 showed negative values (greater tendency for negative trend abrupt changes). A similar pattern, except for C6 that showed a positive median, can be observed for SPI-24. Moreover, the interquartile ranges (IQR) were very small for SPI-1. In contrast, they exhibited broader values ranging between 46% and 72% for time scales equal to or greater than six months. The narrower IQRs observed for SPI-1 suggest that most data points are closely together and that there are fewer outliers or extreme values compared to higher time scales.

The seasonal abrupt changes showed different patterns compared to the trend. In particular, the SPI with time scale between 12 and 24 months showed median values close to 0. Conversely, SPI with a time scale between 1 and 6 months showed negative values for the central-southern clusters C1, C2, and C3. Positive values were observed for the remaining clusters, except for SPI-3, which showed negative median values for C4 and C6. The IQRs were nearly negligible for SPI with a time scale between 12 and 24 months, except for C6 with SPI-24. In contrast, SPI-3 and SPI-6 exhibited broader IQRs, ranging between 17% and 34%. For SPI-1, IQRs ranged between

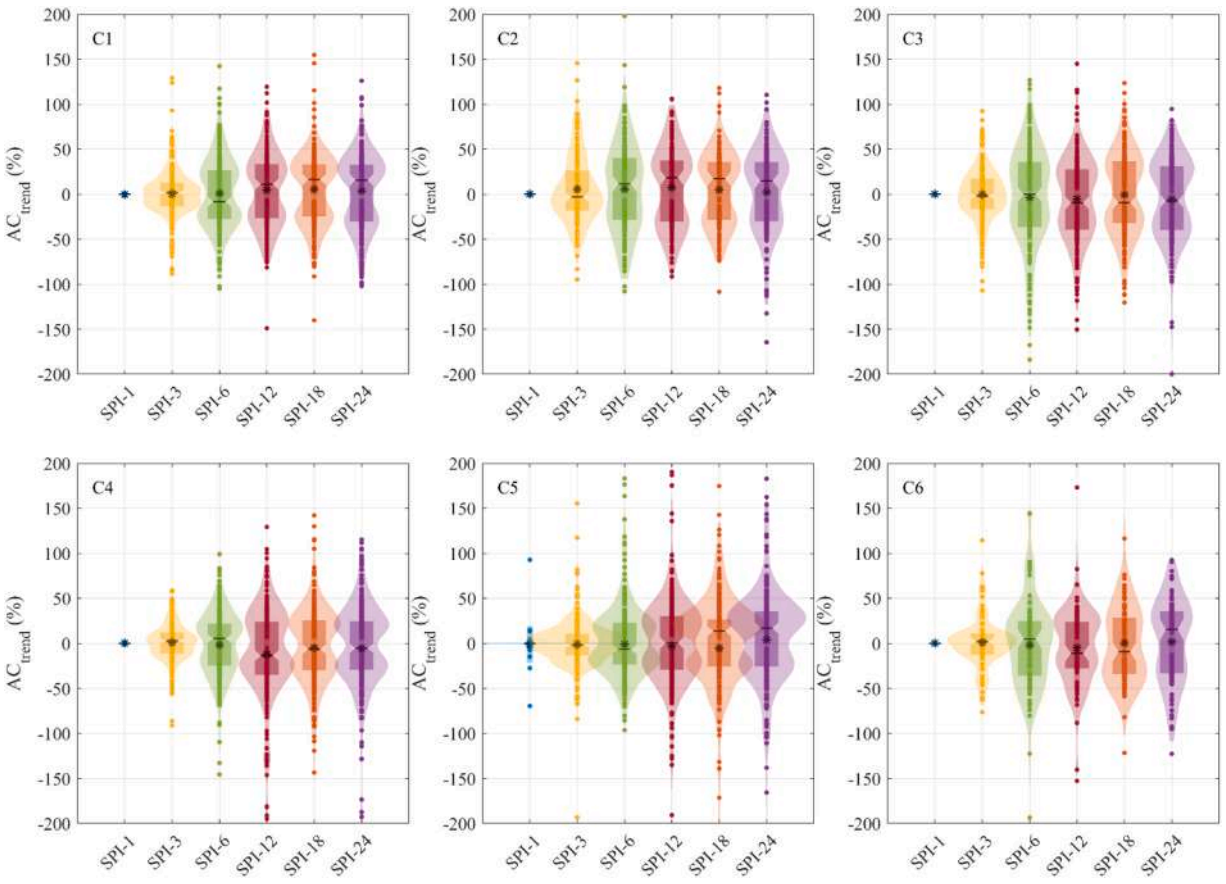

Fig. 7. Combined box and violin plots of the trend abrupt change for the six clusters.

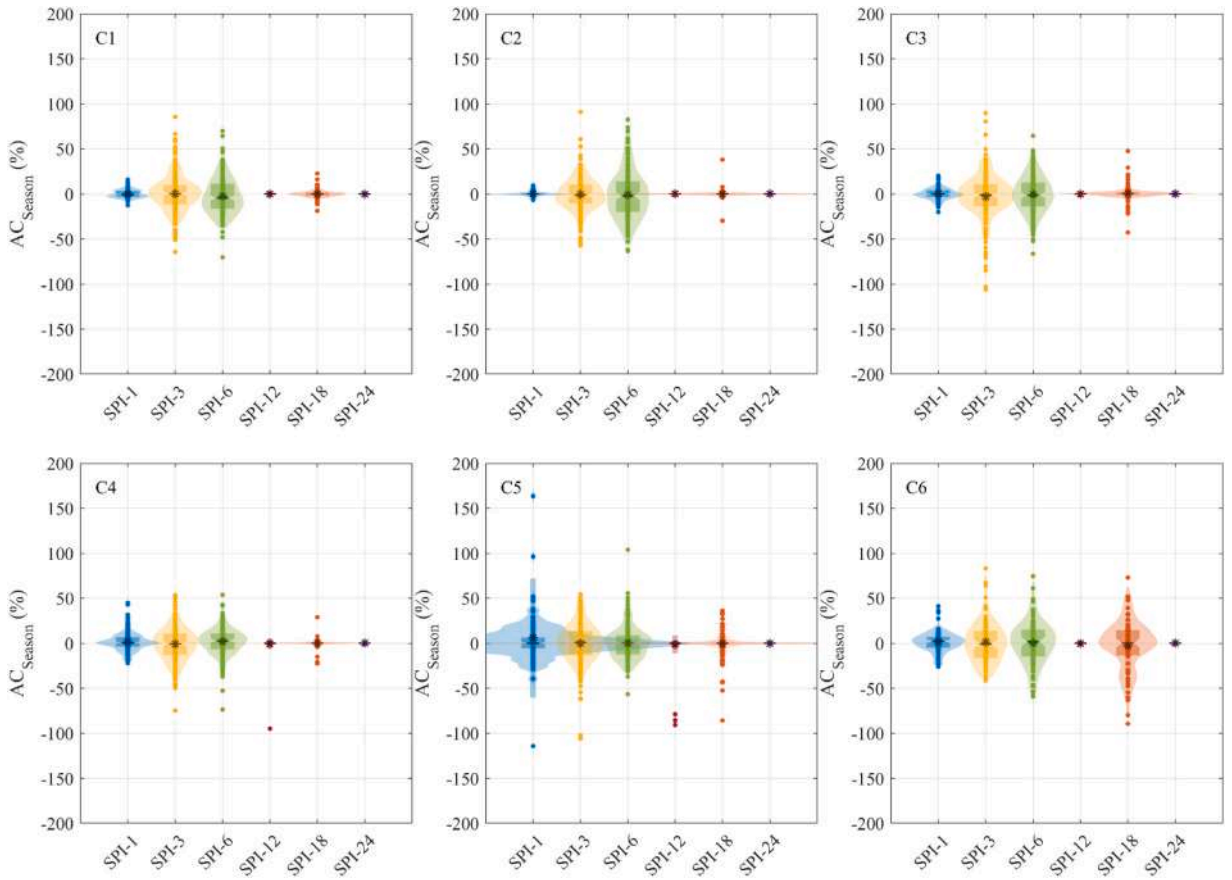

Fig. 8. Combined box and violin plots of the season abrupt change for the six clusters.

1.9% (C2) and 12.1% (C6).

4. Discussion

The extensive study carried out on the SPI at different time scales in the UK allowed the following to be highlighted:

- The approach based on the BEAST and K-means algorithm led to the division of the United Kingdom into six different clusters, generally oriented from south to north, characterized by different SPI patterns.
- The seasonal MK test showed statistically increasing trends across all UK, indicating a climate that is gradually becoming progressively more humid. An exception is represented by cluster C2, southeast of the UK, which, however, exhibits statistically non-significant decreasing trends.
- Regarding the abrupt trend change, the BEAST analysis exhibited an overall increase with increasing SPI time scales, being particularly restrained for SPI-1. Moreover, clusters exhibited significant differences among themselves, with the southern areas that showed, during the first decades, marked positive trend abrupt change (wetter climate) at intermediate SPI time scales, while the northern areas exhibited marked negative trend abrupt change (drier climate) for the same SPI time scales. During the last few decades, the southern clusters also displayed distinct and noticeable positive abrupt changes in trends. However, these changes were not observed in the northern clusters.
- Regarding the seasonal abrupt changes, which can either extend or shorten drought events, the BEAST analysis showed pronounced changes in the earlier decades. However, significant seasonal abrupt changes were still observed during the periods 1980–2000 and 2000–2020, including both positive examples (e.g., SPI-3 for the southern clusters C1 and C2) and negative instances (e.g., for the Northern Ireland cluster C6 for SPI-3 and SPI-6).
- The observed lack of a significant correlation between abrupt seasonal changes and abrupt changes in trends, despite both being assessed across various SPI time scales, highlights the intricate and multifaceted nature of hydrological dynamics. This can be attributed to different aspects. In particular, while both seasonality and trends are examined across SPI time scales from SPI-1 to SPI-24, their fundamental temporal characteristics differ. Seasonality captures cyclic patterns within shorter time intervals, such as monthly or seasonal variations, whereas trends encompass long-term movements over extended periods. The diverse time scales

contribute to the lack of a consistent correlation between abrupt changes in seasonality and trends. Moreover, seasonal changes are often influenced by cyclical factors, such as precipitation variations and temperature fluctuations within a year. On the other hand, trends are driven by broader, overarching factors, including climate change, land use alterations, and shifts in regional hydrology. The dissimilarity in the influencing factors for seasonality and trends contributes to their independence, leading to non-correlation in abrupt changes. In addition, hydrological units within clusters can exhibit unique responses to seasonal and trend changes. In particular, the spatial heterogeneity of climate, topography and land use can contribute to localized effects, with variations in timing and magnitude of seasonal and trend changes.

The clustering performed in the present study was compared with those performed for the UK by Tanguy et al. (2021). The authors performed the clustering based on the K-means algorithm, to monthly series of gridded precipitation (period 1862–2015), dividing the UK in three different clusters: South-East (SE), North-West (NW), or a "Transition" region. Then, the authors computed the SPI for time scales equal to 3, 6, 12 and 24 months. A frequency analysis of drought characteristics revealed regional differences. Short and less severe droughts were more frequent in the NW for shorter accumulation periods (3, 6, and 12 months), while the SE experienced more frequent long, spatially extended, and severe droughts. However, for longer accumulation periods (24 months), fewer distinctions were observed between the NW and SE. The "Transition" region showed lower frequency of severe droughts compared to the other two regions. There are discrepancies between the present study and that of Tanguy et al. (2021). In fact, although both papers used K-means for clustering, in Tanguy et al. (2021) they considered rainfall gridded data as input, whereas in the present paper the outcomes of the BEAST analysis on the SPI time series, such as abrupt changes in trends and seasonality, were taken into account. This led to a division of the UK into six clusters instead of three as in Tanguy et al. (2021). Overall, applying K-means to a subset of parameters obtained from the BEAST analysis, which captures abrupt changes in trend and seasonality, may offer several advantages over considering the original data. The first is the dimensionality reduction, with the BEAST analysis that generates a subset of parameters that summarizes the main features investigated in the present study. As a consequence, the subset of parameters from BEAST may highlight specific aspects of the SPI data that are more sensitive to abrupt changes in trend and seasonality, detecting novel insights into the temporal evolution of drought patterns. K-means applied to this focused subset might result in more distinct clusters, enhancing the model's sensitivity to key patterns. Another aspect is the possible noise reduction. By focusing on parameters obtained from BEAST, the analysis may inherently filter out noise or less relevant information present in the original SPI data. This can lead to more robust cluster assignments and interpretations.

The results of the present study were also compared with those of recent similar work. Although the application of the BEAST algorithm for the identification of changepoints in the UK is something absolutely new, there are some studies in literature on SPI trends. Among these, Vicente-Serrano et al. (2021) analyzed long-term (1851–2018) variability and trends in droughts across Western Europe (including UK) using the SPI index, at time scale of 3 and 12 months, using the MK test. The authors showed statistically significant positive trends (wetter conditions) are over the British and Irish Isles, in agreement with the present study, while negative trends (drier conditions) predominate over Italy and Balkans.

Jaagus et al. (2022) investigated drought conditions in central and eastern Europe from 1949 to 2018, based on SPI and SPEI indices and on the MK test. The authors showed statistically significant increase in SPI and SPEI during the cold season (November-March), highlighting a precipitation increase in the northern part of the study region, in Estonia, Latvia, Lithuania, northern Belarus and northern Poland. The authors also showed how the use of SPEI instead of SPI generally enhances drying trends.

Nevertheless, an essential insight gained from the present study, and from the comparison with existing literature, is the limitation of information derived from the MK test, which, although offers a precise and reliable estimation of overall long-term trends, does not enable the detection of more or less abrupt changes in the investigated variables over the time series. In the context of drought events, this is a crucial aspect because the rapid transition from a state of humidity to drought has significant practical implications for agriculture and water resources. Indeed, for the present study, in contrast to the seasonal MK test, the BEAST analysis revealed a considerably more variable situation. Clusters like C4, which had indicated pronounced positive trends according to the MK test, also exhibited notable negative abrupt changes in trends for various decades. This confirms that, despite a trend towards a wetter climate, abrupt changes in trends are quite common, with drought events characterized by irregular seasonality that can affect the different areas of the UK.

Overall, the BEAST algorithm proved to be aa reliable tool for drought trend analysis due to its ability to handle non-stationary time series, accommodating varying drought patterns. Its Bayesian framework provides robust uncertainty estimates, crucial for reliable changepoint identification in climatic data. Unlike traditional methods, like for example the Pettitt's Test which detects a single changepoint in the time series by comparing the cumulative sums of data values before and after a potential changepoint, BEAST offers flexibility in modeling diverse trends and seasonality at multiple time scales, enhancing its adaptability to complex drought dynamics.

The study's identification of distinct regional drought patterns and significant abrupt changes provides critical insights for early warning systems. Understanding the spatial and temporal variation of drought patterns revealed by this study is pivotal for enhancing the efficacy of early warning systems. By tailoring alerts to specific clusters identified through the BEAST and K-means algorithm, authorities can provide more targeted and accurate information to regions facing distinct drought challenges. The observed positive and negative trend changes underscore the necessity for adaptable strategies within early warning frameworks. Incorporating these findings allows for a more dynamic and responsive approach, ensuring that early warnings reflect the evolving nature of drought conditions. This adaptability is crucial for optimizing preparedness and response measures, as it enables stakeholders to anticipate and mitigate the diverse impacts of drought scenarios across the United Kingdom.

Moreover, agricultural planners and water resource managers can leverage the study's insights for strategic decision-making. The identified clusters provide localized information on SPI patterns, guiding agricultural planners in crop selection and irrigation

planning tailored to each region's specific drought characteristics. For instance, southern clusters exhibiting marked positive trend abrupt changes may indicate a climate becoming wetter, influencing crop choices that thrive in higher moisture conditions. Conversely, northern clusters with marked negative trend abrupt changes may suggest a drier climate, prompting planners to consider drought-resistant crops and more efficient irrigation practices.

The study encountered certain challenges and limitations in the application of the different algorithms. The K-means algorithm assumes homogeneity within clusters, which might not fully capture the complexity of regional drought patterns. Certain regions may exhibit diverse sub-patterns that are overlooked in a homogenous clustering approach. However, the Silhouette score allows this type of problem to be handled, as a high Silhouette still indicates a strong belonging of an area to a given cluster.

More in general, the accuracy of the analysis heavily relies on the quality of input data. Incomplete or inaccurate precipitation data may introduce biases in the results, affecting the reliability of identified trends, abrupt changes and clusters.

In addition, applying the BEAST algorithm, K-means clustering and the seasonal MK test at different time scales requires careful consideration of scale effects. Challenges may arise in maintaining consistency and comparability across scales. However, for the present case study, the arrangement and structure of the clusters does not change as the SPI time scale increases. This stability implies that the spatial organization of drought characteristics, as captured by the clusters, exhibits consistency even when analyzing at different temporal resolutions.

Within the context of climate change, it is possible to argue that pairing trend analysis methods such as Mann-Kendall with changepoint detection algorithms like BEAST can be highly valuable in providing a more comprehensive characterization of the hydrological phenomena under investigation. From this perspective, potential future applications may encompass the analysis of river flows and groundwater levels, both of which can undergo abrupt and sudden fluctuations over seasons or years due to a variety of natural and human-induced factors. Moreover, despite the extensive geographical coverage of the study, the climatic and meteorological conditions across various regions of the UK do not exhibit significant diversity and differ notably from warmer climates. In this context, future research testing this methodology in semi-arid and Mediterranean regions, where the seasonal SPI pattern is more distinct than in the UK, could be particularly intriguing. This would make it possible to understand whether the developed approach is also valid for drought analysis in other areas of the world characterized by different problems in terms of water management. Future research should also explore incorporating additional climatic variables, land-use and remote sensing data for a more holistic understanding of drought dynamics. In this context, it could be beneficial to involve functional climatic variables to explore more deeply the direct consequences of drought on agriculture, water resources, and ecosystems.

Advanced approaches, based on hybrid Machine Learning / Deep Learning (ML/DL) algorithms, could be also used in the future in combination with the developed trend analysis methodology, empowering researchers to extract nuanced insights and improve the overall precision of drought assessments. Hybrid ML/DL models excel in recognizing intricate patterns and relationships between exogenous inputs and target variable (Granata et al., 2022, Granata and Di Nunno, 2023), enhancing the identification of trends and abrupt changes. These algorithms offer superior predictive capabilities, allowing accurate forecasting of drought events (Di Nunno et al., 2023a, 2023b).

5. Conclusion

This study proposed an extensive spatio-temporal analysis of SPI in the UK. The dataset encompassed SPI data at various time scales, from 115 hydrological units spanning the UK territory from 1862 to 2022. The K-means algorithm was applied to divide the study area into six homogeneous regions, each characterized by particular SPI features. Then, the seasonal MK test was used to assess the overall trends for each cluster and SPI time scale. Additionally, the BEAST algorithm was employed for the detection of changepoints in trend and season along the SPI time series. The results of the seasonal MK test revealed increasing SPI trends for all clusters, except for cluster C2 in the southeastern region of the UK. In particular, the trends were more marked for higher time scale, resulting in statistically significant findings for all clusters (except C2) for an SPI time scale ranging from 6 to 24 months. On the other hand, C2 showed decreasing trends across all SPI time scales, but these trends were not statistically significant.

While the seasonal MK test provided clear insights into long-term trends indicating a gradual increase in precipitation, the BEAST analysis uncovered a more complex and diverse scenario. This complexity included the identification of sudden and irregular changes in both trend and seasonality, resulting in abrupt transitions from wet to drought conditions. These findings have significant implications for agriculture and water resource management.

In light of these outcomes, the proposed approach emerges as a valuable decision-making tool for water resource management and the strategic planning of infrastructure projects. It demonstrates the capability to detect both long-term trends and short-term changes within individual hydrological units or broader geographical regions, thereby assisting in informed decision-making.

Declarations

- The authors have no relevant financial or non-financial interests to disclose.
- The authors have no competing interests to declare that are relevant to the content of this article.
- All authors certify that they have no affiliations with or involvement in any organization or entity with any financial interest or non-financial interest in the subject matter or materials discussed in this manuscript.
- The authors have no financial or proprietary interests in any material discussed in this article.

CRediT authorship contribution statement

Fabio Di Nunno: Writing – original draft, Software, Methodology, Investigation, Formal analysis, Data curation, Conceptualization. **Francesco Granata:** Writing – review & editing, Visualization, Validation, Supervision, Methodology, Investigation, Data curation, Conceptualization. **Giovanni de Marinis:** Writing – review & editing, Project administration, Investigation, Funding acquisition.

Declaration of Competing Interest

The authors declare that they have no known competing financial interests or personal relationships that could have appeared to influence the work reported in this paper.

Data availability

Data are available at the following website: https://eip.ceh.ac.uk/hydrology/water-resources.

References

Abahous, H., Ronchail, J., Sifeddine, A., Kenny, L., Bouchaou, L., 2018. Trend and change point analyses of annual precipitation in the Souss-Massa Region in Morocco during 1932–2010. Theor. Appl. Climatol. *134*, 1153–1163.

Aladaileh, H., Al Qinna, M., Karoly, B., Al-Karablieh, E., Rakonczai, J., 2019. An investigation into the spatial and temporal variability of the meteorological drought in Jordan. Climate *7* (6), 82. https://doi.org/10.3390/cli7060082.

Ali, Z., Hussain, I., Faisal, M., Nazir, H.M., Abd-el Moemen, M., Hussain, T., Shamsuddin, S., 2017. A novel multi-scalar drought index for monitoring drought: the standardized precipitation temperature index. Water Resour. Manag. *31*, 4957–4969. https://doi.org/10.1007/s11269-017-1788-1.

Bosneagu, R., Lupu, C.E., Torica, E., Lupu, S., Vatu, N., Tanase, V.M., Vasilache, C., Daneci-Patrau, D., Scurtu, I.C., 2022. Long-term analysis of air temperatures variability and trends on the Romanian Black Sea Coast. Acta Geophys. *70*, 2179–2197.

Cai, Y., Liu, S., Lin, H., 2020. Monitoring the vegetation dynamics in the Dongting lake wetland from 2000 to 2019 using the BEAST algorithm based on dense landsat time series. Appl. Sci. *10* (12), 4209. https://doi.org/10.3390/app10124209.

Callahan, C., Bridge, H., 2021. Data mining of rare alleles to assess biogeographic ancestry. Syst. Inf. Eng. Des. Symp. . (SIEDS) 2021, 1–6. https://doi.org/10.1109/SIEDS52267.2021.9483709.

Costa, A.C., 2011. Local patterns and trends of the Standard Precipitation Index in southern Portugal (1940–1999). Adv. Geosci. *30*, 11–16 adgeo-30-11-2011.

Dadson, S.J., Lopez, H.P., Peng, J., Vora, S., 2019. Hydroclimatic Extremes and Climate Change. Water Science, Policy, and Management: A Global Challenge. Wiley, pp. 11–28.

Demsar, J., Curk, T., Erjavec, A., Gorup, C., Hocevar, T., Milutinovic, M., Mozina, M., Polajnar, M., Toplak, M., Staric, A., Stajdohar, M., Umek, L., Zagar, L., Zbontar, J., Zitnik, M., Zupan, B., 2013. Orange: data mining toolbox in python. J. Mach. Learn. Res. *14* (Aug), 2349–2353.

Derradji, T., Belksier, M.S., Bouznad, I.E., et al., 2023. Spatio-temporal drought monitoring and detection of the areas most vulnerable to drought risk in Mediterranean region, based on remote sensing data (Northeastern Algeria). Arab. J. Geosci. *16* (1) https://doi.org/10.1007/s12517-022-11060-y.

Di Nunno, F., Granata, F., 2023a. Spatio-temporal analysis of drought in Southern Italy: a combined clustering-forecasting approach based on SPEI index and artificial intelligence algorithms. Stoch. Environ. Res. Risk Assess. *37* (6), 2349–2375. https://doi.org/10.1007/s00477-023-02390-8.

Di Nunno, F., Granata, F., 2023b. Future trends of reference evapotranspiration in Sicily based on CORDEX data and machine learning algorithms. Agric. Water Manag. 280, 1–2. https://doi.org/10.1016/j.agwat.2023.108232.

Di Nunno, F., De Matteo, M., Izzo, G., Granata, F., 2023c. A combined clustering and trends analysis approach for characterizing reference evapotranspiration in Veneto. Sustainability *15* (14), 11091. https://doi.org/10.3390/su151411091.

Ghasempour, R., Roushangar, K., Ozgur Kirca, V.S., Demirel, M.C., 2022. Analysis of spatiotemporal variations of drought and its correlations with remote sensing-based indices via wavelet analysis and clustering methods. Hydrol. Res. *53* (1), 175–192. https://doi.org/10.2166/nh.2021.104.

Gholami, H., Moradi, Y., Lotfirad, M., Gandomi, M.A., Bazgir, N., Shokrian Hajibehzad, M., 2022. Detection of abrupt shift and non-parametric analyses of trends in runoff time series in the Dez river basin. Water Supply *22* (2), 1216–1230.

Granata, F., Di Nunno, F., de Marinis, G., 2022. Stacked machine learning algorithms and bidirectional Long Short-Term Memory networks for multi-step ahead streamflow forecasting: a comparative study. J. Hydrol. *613* (1–4), 128431 https://doi.org/10.1016/j.jhydrol.2022.128431.

Granata, F., Di Nunno, F., 2023. Neuroforecasting of daily streamflows in the UK for short- and medium-term horizons: a novel insight. J. Hydrol. *624* (2) https://doi.org/10.1016/j.jhydrol.2023.129888.

Gumus, V., Simsek, O., Avsaroglu, Y., et al., 2021. Spatio-temporal trend analysis of drought in the GAP Region, Turkey. Nat. Hazards *109*, 1759–1776. https://doi.org/10.1007/s11069-021-04897-1.

Guo, H., Bao, A., Liu, T., Jiapaer, G., Ndayisaba, F., Jiang, L., Kurban, A., De Maeyer, P., 2018. Spatial and temporal characteristics of droughts in Central Asia during 1966-2015. Sci. Total Environ. *624*, 1523–1538. https://doi.org/10.1016/j.scitotenv.2017.12.120.

Hirsch, R.M., Slack, J.R., 1984. A nonparametric trend test for seasonal data with serial dependence. Water Resour. Res. *20* (6), 727–732. https://doi.org/10.1029/WR020i006p00727.

Hollis, D., McCarthy, M.P., Kendon, M., Legg, T., Simpson, I., 2019. HadUK-Grid—A new UK dataset of gridded climate observations. Geosci. Data J. *6*, 151–159. https://doi.org/10.1002/gdj3.78.

Hu, T., Toman, E.M., Chen, G., Shao, G., Zhou, Y., Li, Y., Zhao, K., Feng, Y., 2021. Mapping fine-scale human disturbances in a working landscape with Landsat time series on Google Earth Engine. ISPRS J. Photogramm. Remote Sens. 176, 250–261. https://doi.org/10.1016/j.isprsjprs.2021.04.008.

Jaagus, J., Aasa, A., Aniskevich, S., Boincean, B., Bojariu, R., Briede, A., Danilovich, I., Castro, F.D., Dumitrescu, A., Labuda, M., Labudová, L., Lõhmus, K., Melnik, V., Mõisja, K., Pongracz, R., Potopová, V., Řezníčková, L., Rimkus, E., Semenova, I., Stonevičius, E., Štěpánek, P., Trnka, M., Vicente-Serrano, S.M., Wibig, J., Zahradníček, P., 2022. Long-term changes in drought indices in eastern and central Europe. Int. J. Climatol. *42* (1), 225–249. https://doi.org/10.1002/joc.7241.

Jarušková, D., 1997. Some problems with application of changepoint detection methods to environmental data. Environmetrics *8* (5), 469.483.

Keerthana, A., Nair, A., 2022. Trend Analysis of Hydro-Climatological Factors Using a Bayesian Ensemble Algorithm with Reasoning from Dynamic and Static Variables. Atmosphere 13 (12), 1961. https://doi.org/10.3390/atmos13121961.

Keller, V.D.J., Tanguy, M., Prosdocimi, I., Terry, J.A., Hitt, O., Cole, S.J., et al., 2015. CEH-GEAR: 1 km resolution daily and monthly areal rainfall estimates for the UK for hydrological and other applications. Earth Syst. Sci. Data *7*, 143–155. https://doi.org/10.5194/essd-7-143-2015.

Kendall, M.G., 1948. Rank correlation methods. Griffin 202.

Khan, A.A., Zhao, Y., khan, J., et al., 2021. Spatial and Temporal Analysis of Rainfall and Drought Condition in Southwest Xinjiang in Northwest China, Using Various Climate Indices. Earth Syst. Environ. *5*, 201–216. https://doi.org/10.1007/s41748-021-00226-5.

Kral, F., Fry, M. and Dixon, H. (2015). Integrated Hydrological Units of the United Kingdom: Hydrometric Areas without Coastline. NERC Environmental Information Data Centre, doi: 10.5285/3a4e94fc-4c68-47eb-a217-adee2a6b02b3.

Legouhy, A. (2023). al_goodplot - boxblot & violin plot (⟨https://www.mathworks.com/matlabcentral/fileexchange/91790-al_goodplot-boxblot-violin-plot⟩), MATLAB Central File Exchange. Retrieved August 3, 2023.
Li, B., Su, H., Chen, F., Li, S., Tian, J., Qin, Y., Zhang, R., Chen, S., Yang, Y., Rong, Y., 2013. The changing pattern of droughts in the Lancang River Basin during 1960-2005. Theor. Appl. Climatol. 111 (3-4), 401–415. https://doi.org/10.1007/s00704-012-0658-2.
Liu, Y., Zhu, Y., Ren, L., Singh, V.P., Yang, X., Yuan, F., 2017. A multiscalar Palmer drought severity index. Geophys. Res. Lett. *44* (13), 6850–6858. https://doi.org/10.1002/2017gl073871.
Lombard, F., 1987. Rank tests for changepoint problems. Biometrika *74* (3), 615–624.
Mann, H.B., 1945. Nonparametric tests against trend. Econometrica *13* (3), 245–259.
McKee, T.B., Doesken, N.J., Kleist, J., 1993. The relationship of drought frequency and duration to time scales. Preprints, Eighth Conf. on Applied Climatology. Anaheim, CA. Am. Meteorol. Soc. 179–184.
Neto, R.M.B., Santos, C.A.G., da Silva, R.M., dos Santos, C.A.C., Liu, Z., Quinn, N.W., 2021. Geospatial cluster analysis of the state, duration and severity of drought over Paraíba State, northeastern Brazil. Sci. Total Environ. *799*, 149492 https://doi.org/10.1016/j.scitotenv.2021.149492.
Palmer, W.C., 1965. Meteorological droughts. U. S. Dep. Commer., Weather Bur. Res. *Paper*, *45*, 58.
Perry, M., Hollis, D., 2005. The generation of monthly gridded datasets for a range of climatic variables over the UK. Int. J. Climatol. *25*, 1041–1054. https://doi.org/10.1002/joc.1161.
Pettitt, A.N., 1979. A non-parametric approach to the changepoint problem. J. R. Stat. Soc.: Ser. C. (Appl. Stat.) *28* (2), 126–135.
Reeves, J., Chen, J., Wang, X.L., Lund, R., Lu, Q.Q., 2007. A review and comparison of changepoint detection techniques for climate data. J. Appl. Meteorol. Climatol. *46* (6), 900–915.
Roushangar, K. and Ghasempour, R. (2021). Multi-temporal analysis for drought classifying based on SPEI gridded data and hybrid maximal overlap discrete wavelet transform. International journal of Environmental Science and Technology.
Sakizadeh, M., Milewski, A., Sattari, M.T., 2023. Analysis of Long-Term Trend of Stream Flow and Interaction Effect of Land Use and Land Cover on Water Yield by SWAT Model and Statistical Learning in Part of Urmia Lake Basin, Northwest of Iran. Water *15*, 690. https://doi.org/10.3390/w15040690.
Sen, P.K., 1968. Estimates of the regression coefficient based on Kendall's tau. J. Am. Stat. Assoc. *63* (324), 1379–1389.
Shahfahad, Talukdar, S., Ghose, B., et al., 2023. Predicting long term regional drought pattern in Northeast India using advanced statistical technique and wavelet-machine learning approach. Model. Earth Syst. Environ. https://doi.org/10.1007/s40808-023-01818-y.
Stagge, J.H., Tallaksen, L.M., Gudmundsson, L., Van Loon, A.F., Stahl, K., 2015. Candidate Distributions for Climatological Drought Indices (SPI and SPEI). Int. J. Climatol. https://doi.org/10.1002/joc.4267.
Tan, C., Yang, J., Li, M., 2015. Temporal-spatial variation of drought indicated by SPI and SPEI in Ningxia Hui autonomous region China. Atmosphere *6* (10), 1399–1421. https://doi.org/10.3390/atmos6101399.
Tanguy, M., Fry, M., Svensson, C., Hannaford, J., 2017. Historic Standardised Precipitation Index time series for IHU Hydrometric Areas (1862-2015) v2. NERC Environ. Inf. Data Cent. https://doi.org/10.5285/a754cae2-d6a4-456e-b367-e99891d7920f.
Tanguy, M., Dixon, H., Prosdocimi, I., Morris, D.G., and Keller, V.D.J. (2019). Gridded Estimates of Daily and Monthly Areal Rainfall for the United Kingdom (1890-2017) [CEH-GEAR]. Atlanta, GE: NERC Environmental Information Data Centre.
Tanguy, M., Haslinger, K., Svensson, C., Parry, S., Barker, L.J., Hannaford, J., Prudhomme, C., 2021. Regional Differences in Spatiotemporal Drought Characteristics in Great Britain. Front. Environ. Sci. *9*, 639649 https://doi.org/10.3389/fenvs.2021.639649.
The MathWorks Inc. Optimization Toolbox version: 9.0.13 (R2022b), Natick, Massachusetts: The MathWorks Inc. 2022 https://www.mathworks.com.
Vicente-Serrano, S.M., Begueria, S., Lopez-Moreno, J.I., 2010. A multiscalar drought index sensitive to global warming: the standardized precipitation evapotranspiration index. J. Clim. *23* (7), 1696–1718.
Vicente-Serrano, S.M., Domínguez-Castro, F., Murphy, C., et al., 2021. Long-term variability and trends in meteorological droughts in Western Europe (1851–2018). E690-E717 Int. J. Climatol. 41 (Suppl. 1). https://doi.org/10.1002/joc.6719.
Wells, N., Goddard, S., Michaelsen, J., 2004. A self-calibrating palmer drought severity index. J. Clim. *17*, 2335–2351. https://doi.org/10.1175/1520-0442(2004)017<2335:ASPDSI>2.0.CO;2.
Wu, G., Chen, J., Shi, X., Kim, J.-S., Xia, J., Zhang, L., 2022. Impacts of global climate warming on meteorological and hydrological droughts and their propagations. Earth'S. Future *10*, e2021EF002542. https://doi.org/10.1029/2021EF002542.
Xu, X., Yang, J., Ma, C., Qu, X., Chen, J., Cheng, L., 2022. Segmented modeling method of dam displacement based on BEAST time series decomposition. Measurement *202*, 111811. https://doi.org/10.1016/j.measurement.2022.111811.
Yoo, J., Kwon, H.H., Kim, T.W., Ahn, J.H., 2012. Drought frequency analysis using cluster analysis and bivariate probability distribution (pp). J. Hydrol. 420-421, 102–111. https://doi.org/10.1016/j.jhydrol.2011.11.046.
Zerouali, B., Pawar, U.V., Elbeltagi, A., et al., 2023. Change-point detection in monsoon rainfall of Narmada River (central India) during 1901–2015. J. Earth Syst. Sci. *132*, 133. https://doi.org/10.1007/s12040-023-02140-y.
Zhang, G., Su, X., Singh, V.P., Ayantobo, O.O., 2021. Appraising standardized moisture anomaly index (SZI) in drought projection across China under CMIP6 forcing scenarios. J. Hydrol.: Reg. Stud. *37*, 100898 https://doi.org/10.1016/j.ejrh.2021.100898.
Zhang, Q., Li, J., Singh, V.P., et al., 2012. SPI-based evaluation of drought events in Xinjiang, China. Nat. Hazards *64*, 481–492. https://doi.org/10.1007/s11069-012-0251-0.
Zhao, K., Wulder, M.A., Hu, T., Bright, R., Wu, Q., Qin, H., Li, Y., Toman, E., Mallick, B., Zhang, X., Brown, M., 2019. Detecting change-point, trend, and seasonality in satellite time series data to track abrupt changes and nonlinear dynamics: A Bayesian ensemble algorithm. Remote Sens. Environ. *232*, 111181 https://doi.org/10.1016/j.rse.2019.04.034.